SIAM J. SCI. COMPUT.
Vol. 43, No. 6, pp. B1164–B1197

MINIMUM PRINCIPLE ON SPECIFIC ENTROPY AND HIGH-ORDER ACCURATE INVARIANT-REGION-PRESERVING NUMERICAL METHODS FOR RELATIVISTIC HYDRODYNAMICS*

KAILIANG WU†

Abstract. This paper first explores Tadmor's minimum entropy principle for the special relativistic hydrodynamics (RHD) equations and incorporates this principle into the design of robust high-order discontinuous Galerkin (DG) and finite volume schemes for RHD on general meshes. The proposed schemes are rigorously proven to preserve numerical solutions in a global *invariant region* constituted by all the known intrinsic constraints: minimum entropy principle, the subluminal constraint on fluid velocity, the positivity of pressure, and the positivity of rest-mass density. Relativistic effects lead to some essential difficulties in the present study which are not encountered in the nonrelativistic case. Most notably, in the RHD case the specific entropy is a highly nonlinear *implicit* function of the conservative variables, and, moreover, there is also no explicit formula of the flux in terms of the conservative variables. In order to overcome the resulting challenges, we first propose a novel *equivalent* form of the invariant region by skillfully introducing two auxiliary variables. As a notable feature, all the constraints in the novel form are *explicit* and *linear* with respect to the conservative variables. This provides a highly effective approach to theoretically analyze the invariant-region-preserving (IRP) property of numerical schemes for RHD, *without any assumption on the IRP property of the exact Riemann solver*. Based on this, we prove the convexity of the invariant region and establish the generalized Lax–Friedrichs splitting properties via technical estimates, laying the foundation for our rigorous IRP analyses. It is rigorously shown that the first-order Lax–Friedrichs type scheme for the RHD equations satisfies a local minimum entropy principle and is IRP under a CFL condition. Provably IRP high-order accurate DG and finite volume methods are then developed for the RHD with the help of a simple scaling limiter, which is designed by following the bound-preserving type limiters in the literature. Several numerical examples demonstrate the effectiveness and robustness of the proposed schemes.

Key words. minimum entropy principle, invariant region, bound-preserving, relativistic hydrodynamics, discontinuous Galerkin, finite volume, high-order accuracy

AMS subject classifications. 35L65, 65M60, 65M08, 65M12, 76Y05

DOI. 10.1137/21M1397994

1. Introduction.

In the study of the fluid dynamics, when the fluid flow moves close to the speed of light or when sufficiently strong gravitational fields are involved, the special or general relativistic effect has to be taken into account accordingly. Relativistic hydrodynamics (RHD) plays an important role in a wide range of applications, e.g., astrophysics and high energy physics, and has been applied to investigate astrophysical scenarios ranging from stellar to galactic scales.

In the framework of special relativity, the motion of ideal relativistic fluid is governed by the conservation of mass density D, momentum $\mathbf{m}$, and energy E. In the laboratory frame, the d-dimensional special RHD equations can be written into

*Submitted to the journal's Computational Methods in Science and Engineering section February 9, 2021; accepted for publication (in revised form) August 31, 2021; published electronically November 23, 2021.

https://doi.org/10.1137/21M1397994

Funding: The author was partially supported by the National Natural Science Foundation of China, project 12171227.

†Department of Mathematics, Southern University of Science and Technology, Shenzhen, Guangdong, 518055, People's Republic of China (wukl@sustech.edu.cn).

the following nonlinear hyperbolic system:

$$\frac{\partial \mathbf{U}}{\partial t} + \sum_{i=1}^{d} \frac{\partial \mathbf{F}_i(\mathbf{U})}{\partial x_i} = \mathbf{0}, \tag{1.1}$$

with the conservative vector $\mathbf{U}$ and the flux $\mathbf{F}_i$ defined by

$$\mathbf{U} = (D,\ \boldsymbol{m}^\top,\ E)^\top = (\rho W,\ \rho h W^2 \boldsymbol{v}^\top,\ \rho h W^2 - p)^\top, \tag{1.2}$$

$$\mathbf{F}_i = (D v_i,\ v_i \boldsymbol{m}^\top + p\mathbf{e}_i^\top,\ m_i)^\top = (\rho W v_i,\ \rho h W^2 v_i \boldsymbol{v}^\top + p\mathbf{e}_i^\top,\ \rho h W^2 v_i)^\top, \tag{1.3}$$

where, and hereafter, the geometrized unit system is employed so that the speed of light in vacuum $c = 1$. In (1.2)–(1.3), ρ denotes the rest-mass density, p is the thermal pressure, the column vector $\boldsymbol{v} = (v_1, \ldots, v_d)^\top$ represents the velocity field of the fluid, $W = 1/\sqrt{1 - \|\boldsymbol{v}\|^2}$ denotes the Lorentz factor with $\|\cdot\|$ denoting the vector 2-norm, $h = 1 + e + \frac{p}{\rho}$ stands for the specific enthalpy with e being the specific internal energy, and the row vector $\mathbf{e}_i$ denotes the ith column of the identity matrix of size d. To close the system (1.1), an equation of state (EOS) is needed. We focus on the ideal EOS: $p = (\Gamma - 1)\rho e$ with the constant $\Gamma \in (1, 2]$ being the adiabatic index, for which the restriction $\Gamma \le 2$ is required by compressibility assumptions and the relativistic causality (cf. [34]).

As we can see from (1.2)–(1.3), the conservative vector $\mathbf{U}$ and the flux $\mathbf{F}_i$ are explicitly expressed in terms of the primitive quantities $\mathbf{V} := (\rho, \boldsymbol{v}^\top, p)^\top$. However, unlike the nonrelativistic case, for RHD there are no explicit formulas for either the flux $\mathbf{F}_i$ or the primitive vector $\mathbf{V}$ in terms of $\mathbf{U}$. Therefore, in order to evaluate the flux $\mathbf{F}_i(\mathbf{U})$ in the computations, one first has to perform the inverse transformation of (1.2) from the conservative quantities $\mathbf{U}$ to the primitive quantities $\mathbf{V}$. Given a conservative vector $\mathbf{U} = (D, \boldsymbol{m}^\top, E)^\top$, we can compute the values of the corresponding primitive quantities $\{p(\mathbf{U}), \boldsymbol{v}(\mathbf{U}), \rho(\mathbf{U})\}$ as follows: First, solve the nonlinear algebraic equation

$$\frac{\|\boldsymbol{m}\|^2}{E + p} + D\sqrt{1 - \frac{\|\boldsymbol{m}\|^2}{(E + p)^2}} + \frac{p}{\Gamma - 1} - E = 0, \qquad p \in [0, +\infty), \tag{1.4}$$

by utilizing a root-finding algorithm to get the pressure $p(\mathbf{U})$; then calculate the velocity and rest-mass density by $\boldsymbol{v}(\mathbf{U}) = \boldsymbol{m}/\big(E + p(\mathbf{U})\big)$ and $\rho(\mathbf{U}) = D\sqrt{1 - \|\boldsymbol{v}(\mathbf{U})\|^2}$, respectively. Both the physical significance and the hyperbolicity of (1.1) require that the constraints

$$\rho > 0, \quad p > 0, \quad \|\boldsymbol{v}\| < c = 1, \tag{1.5}$$

always hold. In other words, the conservative vector $\mathbf{U}$ must stay in the admissible state set

$$\mathcal{G} := \left\{ \mathbf{U} = (D, \boldsymbol{m}^\top, E)^\top \in \mathbb{R}^{d+2} :\ \rho(\mathbf{U}) > 0,\ p(\mathbf{U}) > 0,\ \|\boldsymbol{v}(\mathbf{U})\| < 1 \right\}, \tag{1.6}$$

where the functions $\rho(\mathbf{U})$, $p(\mathbf{U})$, and $\boldsymbol{v}(\mathbf{U})$ are highly nonlinear and have no explicit formulas, as defined above. It was observed in [23] and rigorously proven in [34, Lemma 2.1] that the set $\mathcal{G}$ is convex and is exactly *equivalent* to the following set:

$$\mathcal{G}_1 := \left\{ \mathbf{U} = (D, \boldsymbol{m}^\top, E)^\top \in \mathbb{R}^{d+2} :\ D > 0,\ E > \sqrt{D^2 + \|\boldsymbol{m}\|^2} \right\}. \tag{1.7}$$

Moreover, if $\mathbf{U} \in \mathcal{G}_1$, then the nonlinear equation (1.4) has a unique positive solution [34].

Because of the nonlinear hyperbolic nature of the system (1.1), discontinuous solutions may develop from even smooth initial data, and weak solutions must therefore be considered. As is well known, weak solutions are not uniquely defined in general; the following inequality, known as the entropy condition, is often adopted as a criterion to select the "physically relevant" solution among all weak solutions:

$$\frac{\partial \mathscr{E}}{\partial t} + \sum_{i=1}^{d} \frac{\partial \mathscr{F}_i}{\partial x_i} \le 0. \tag{1.8}$$

Here (1.8) should be interpreted in the sense of distribution, $\mathscr{E}(\mathbf{U})$ is a strictly convex function of $\mathbf{U}$ and called an entropy function, and $\mathscr{F}_i(\mathbf{U})$ is the associated entropy fluxes such that the relation $\frac{\partial \mathscr{E}}{\partial \mathbf{U}} \frac{\partial \mathbf{F}_i}{\partial \mathbf{U}} = \frac{\partial \mathscr{F}_i}{\partial \mathbf{U}}$ holds. *Entropy solutions* are defined to be weak solutions which in addition satisfy (1.8) for *all entropy pairs* $(\mathscr{E}, \mathscr{F}_i)$. For the (nonrelativistic) gas dynamics equations, Tadmor [27] proved that entropy solutions satisfy a local minimum principle on the specific entropy $S(\boldsymbol{x}, t) = \log\left(p\rho^{-\Gamma}\right)$:

$$S(\boldsymbol{x}, t+\tau) \ge \min\left\{S(\boldsymbol{y}, t) : \ \|\boldsymbol{y} - \boldsymbol{x}\| \le \tau v_{\max}\right\}, \tag{1.9}$$

where $\tau > 0$, and $v_{\max}$ denotes the maximal wave speed. This implies the spatial minimum of the specific entropy, $\min_{\boldsymbol{x}} S(\boldsymbol{x}, t)$, is a *nondecreasing* function of time t, and $S(\boldsymbol{x}, t) \ge \min_{\boldsymbol{x}} S(\boldsymbol{x}, 0)$. (Entropy principles were also shown by Guermond and Popov [8] with viscous regularization of the nonrelativistic Euler equations.) In this paper, we will explore such a minimum entropy principle in the RHD case and prove that it also holds for entropy solutions of (1.1). The entropy principle, along with the intrinsic physical constraints in (1.6), implies a global invariant region for the solution of the RHD equations (1.1) with initial data $\mathbf{U}_0(\boldsymbol{x})$, that is,

$$\Omega_{S_0} := \left\{\mathbf{U} = (D, \boldsymbol{m}^\top, E)^\top \in \mathbb{R}^{d+2} : \ \rho(\mathbf{U}) > 0, \ p(\mathbf{U}) > 0, \ \|\boldsymbol{v}(\mathbf{U})\| < 1, \ S(\mathbf{U}) \ge S_0\right\}, \tag{1.10}$$

where $S_0 := \operatorname{ess\,inf}_{\boldsymbol{x}} S(\mathbf{U}_0(\boldsymbol{x}))$.

It is natural and interesting to explore robust numerical RHD schemes, whose solutions always stay in the invariant region Ω_{S_0}, i.e., they satisfy the minimum entropy principle at the discrete level and also preserve the intrinsic physical constraints (1.5). Note that, to obtain a well-defined specific entropy for the numerical solution, it is necessary to first guarantee the positivity of pressure and rest-mass density. The subluminal constraint on fluid velocity is also crucial for the relativistic causality, as its violation would yield an imaginary Lorentz factor. In fact, violating any of the constraints (1.5) will cause numerical instability and the breakdown of the computation. Therefore, the preservation of the minimum entropy principle should be considered together with the constraints (1.5). Recent years have witnessed some advances in developing high-order numerical schemes, which provably preserve the constraints (1.5), for the special RHD [34, 24, 37] and the general RHD [28]. Those works were motivated by [40, 41, 38, 14] on bound-preserving high-order schemes for scalar conservation laws and the nonrelativistic Euler equations. More recently, constraint-preserving schemes were also developed for the special relativistic magnetohydrodynamics (RMHD) [36, 33], as extension of the positivity-preserving MHD schemes [29, 30, 31]. In addition, a flux-limiting approach which preserves the positivity of the rest-mass density was designed in [25]. A reconstruction technique was proposed in [1] to enforce the subluminal constraint on fluid velocity. A flux-limiting

entropy-viscosity approach was developed in [6] for RHD, based on a measure of the entropy generated by the solution. A comprehensive review of numerical RHD schemes is beyond the scope of the present paper; we refer interested readers to the review articles [21, 22] and a limited list of some recent works [13, 44, 35, 3, 2, 32] as well as references therein. Yet, up to now, there is still no work that studied the minimum entropy principle for the RHD system (1.1) at either the PDE level or the numerical level, and high-order schemes which preserve the invariant region (1.10) have *not* yet been developed for RHD.

For the nonrelativistic counterparts such as the Euler system, the minimum entropy principle and invariant-region-preserving (IRP) numerical schemes have been well studied in the literature. Tadmor [27] discovered (1.9) and proved, for the equations of the nonrelativistic gas dynamics, that first-order approximations such as the Godunov and Lax–Friedrichs (LF) schemes satisfy a minimum entropy principle. Using a slope reconstruction with limiter, Khobalatte and Perthame [18] developed second-order kinetic schemes that preserve a discrete minimum principle for the specific entropy. It was also observed in [18] that enforcing the discrete minimum entropy principle could help to damp numerical oscillations near the discontinuities. Zhang and Shu [42] proposed a framework of enforcing the minimum entropy principle for high-order discontinuous Galerkin (DG) and finite volume schemes, by extending their high-order positivity-preserving schemes [41, 43], for the nonrelativistic gas dynamics equations. The resulting high-order schemes in [42] were proven to preserve a discrete minimum entropy principle and the positivity of density and pressure under a condition accessible by a simple bound-preserving limiter without destroying the high-order accuracy. Lv and Ihme [20] proposed an entropy-bounded DG scheme for the Euler equations on arbitrary meshes. Guermond, Popov, and their collaborators (cf. [9, 10, 7, 11]) developed the IRP approximations in the context of continuous finite elements with convex limiting for solving general hyperbolic systems including the Euler system. Jiang and Liu proposed new IRP limiters for the DG methods solving the isentropic Euler system [17], the compressible Euler system [15], and general multidimensional hyperbolic conservation laws [16]. Gouasmi et al. [5] proved a minimum entropy principle on entropy solutions to the compressible multicomponent Euler system at the smooth and discrete levels.

The aim of this paper is twofold. First, we show that the minimum entropy principle (1.9), which was originally demonstrated by Tadmor [27] for the (nonrelativistic) gas dynamics, is also valid for the RHD equations (1.1) with the ideal EOS. A key point in the present study is to prove a condition on smooth function $\mathcal{H}(S)$ such that the entropy function $\mathscr{E}(\mathbf{U}) = -D\mathcal{H}(S)$ is strictly convex. Our second goal is to develop high-order accurate IRP DG and finite volume methods which provably preserve the numerical solutions in the invariant region Ω_{S_0}, i.e., preserve a discrete minimum entropy principle and the intrinsic physical constraints (1.5). In fact, achieving these two goals is nontrivial. Due to the nonlinearity and the implicit form of the function $S(\mathbf{U})$, it is hard to study the convexity of the entropy function $\mathscr{E}(\mathbf{U})$ in the RHD case; see Proposition 2.1. Also, analytically judging whether an arbitrarily given state $\mathbf{U}$ belongs to Ω_{S_0} is already a difficult task; it is more challenging to design and analyze numerical schemes that provably preserve the solutions in Ω_{S_0}. We will address the difficulties via a novel *equivalent* form of the invariant region; see Theorem 3.3. As a notable feature, all the constraints in the novel form are *explicit* and *linear* with respect to the conservative variables. This provides a highly effective approach to theoretically analyze the IRP property of RHD schemes. Based on this, we will prove the convexity of the invariant region (section 3.2) and establish the generalized LF split-

ting properties via highly technical estimates (section 3.3), which lay the foundation for analyzing our IRP schemes in sections 4–5. The high-order accurate IRP schemes are constructed with the aid of a simple scaling limiter, which is designed by following the bound-preserving type limiters and frameworks in the literature [41, 42, 24, 16, 37].

It is worth noting that the proposed numerical IRP analysis approach has some *essential and significant differences* compared to those in the literature (cf. [42, 9, 7, 16]). For example, some standard analyses on the IRP properties of numerical schemes often relied on invoking the IRP property of the exact Riemann solver for the studied equations, while our IRP analyses do *not* require any assumption on the IRP property of the exact Riemann solver.[1] Instead, we directly prove the IRP properties of the LF approximate Riemann solver and numerical schemes with the LF flux by using our novel equivalent form of the invariant region and the generalized LF splitting properties. Thus our analysis approach can be potentially extensible to some other complicated physical systems for which the exact Riemann solver is not easily available or generally not IRP (e.g., for multidimensional MHD systems [29, 30, 31, 33] if there is a numerical jump in the parallel magnetic component).

2. Minimum entropy principle at the PDE level.

2.1. Convex entropy functions. Let $\mathcal{H}(S)$ be a function of the specific entropy S. As shown in [2] for $d = 1$, for any smooth function $\mathcal{H}(S)$, the smooth solutions of the RHD equations (1.1) satisfy

$$\frac{\partial}{\partial t}\Big(-\rho W\mathcal{H}(S)\Big)+\sum_{i=1}^{d}\frac{\partial}{\partial x_i}\Big(-\rho W v_i\mathcal{H}(S)\Big)=0, \tag{2.1}$$

which also holds for the multidimensional cases ($2 \le d \le 3$). In fact, the derivations of (2.1) for $2 \le d \le 3$ are very similar to that for $d = 1$, and we give a unified proof for arbitrary d in section SM1 of the supplementary material for completeness. Equation (2.1) implies that $(\mathscr{E},\mathscr{F}_i) = \big(-D\mathcal{H}(S), -Dv_i\mathcal{H}(S)\big)$ is an entropy–entropy flux pair if $\mathscr{E}(\mathbf{U}) = -D\mathcal{H}(S)$ is a strictly convex function of the conservative variables $\mathbf{U} \in \mathcal{G}$.

It is well known that, for a special choice $\mathcal{H}(S) = S$ or $\mathcal{H}(S) = \frac{S}{\Gamma-1}$, the corresponding $\mathscr{E}(\mathbf{U})$ is a valid entropy function for the RHD; see [6, 2, 3, 32]. However, it is unclear, for a general $\mathcal{H}(S)$, what the condition is on $\mathcal{H}(S)$ such that the corresponding $\mathscr{E}(\mathbf{U})$ is strictly convex. This has not been addressed for the RHD case in the literature and is now explored in the following proposition.

PROPOSITION 2.1. *For a smooth function $\mathcal{H}(S)$, the corresponding $\mathscr{E}(\mathbf{U}) = -D\mathcal{H}(S)$ is a strictly convex entropy function if and only if*

$$\mathcal{H}'(S) > 0, \qquad \mathcal{H}'(S) - \Gamma\mathcal{H}''(S) > 0. \tag{2.2}$$

Proof. We study the convexity of $\mathscr{E}(\mathbf{U})$ by investigating the positive definiteness of the Hessian matrix $\mathscr{E}_{\mathbf{uu}} := \big(\frac{\partial^2\mathscr{E}}{\partial u_i\partial u_j}\big)_{1\le i,j\le d+2}$, where u_i denotes the ith component of $\mathbf{U}$. A straightforward calculation gives $\frac{\partial^2\mathscr{E}}{\partial u_i\partial u_j} = -\mathcal{H}'(S)\big(\frac{\partial D}{\partial u_i}\frac{\partial S}{\partial u_j}+\frac{\partial D}{\partial u_j}\frac{\partial S}{\partial u_i}\big) - D\mathcal{H}''(S)\frac{\partial S}{\partial u_i}\frac{\partial S}{\partial u_j} - D\mathcal{H}'(S)\frac{\partial^2 S}{\partial u_i\partial u_j}$. This implies that

$$\mathscr{E}_{\mathbf{uu}} = -\mathcal{H}'(S)\left(\mathbf{e}_1 S_{\mathbf{u}}^\top + S_{\mathbf{u}}\mathbf{e}_1^\top + DS_{\mathbf{uu}}\right) - D\mathcal{H}''(S)S_{\mathbf{u}}S_{\mathbf{u}}^\top \tag{2.3}$$

[1] It is often reasonable to invoke or assume that the exact Riemann solver preserves the invariant domain. In fact, this is provenly true for a number of other systems, but has not yet been proven for the RHD equations (1.1). Rigorous analysis on the IRP property of the exact Riemann solver, including the preservation of the constraints (1.5), is highly nontrivial.

$$= -\mathcal{H}'(S)\mathbf{A}_1 + \frac{D}{\Gamma}\left(\mathcal{H}'(S) - \Gamma\mathcal{H}''(S)\right) S_{\mathbf{u}} S_{\mathbf{u}}^\top,$$

where $\mathbf{e}_1 = (1, \mathbf{0}_{d+1}^\top)^\top$, $\mathbf{0}_{d+1}$ denotes the zero vector of length $d+1$, and

$$\mathbf{A}_1 := \mathbf{e}_1 S_{\mathbf{u}}^\top + S_{\mathbf{u}}\mathbf{e}_1^\top + D S_{\mathbf{uu}} + \frac{1}{\Gamma} D S_{\mathbf{u}} S_{\mathbf{u}}^\top.$$

Since S cannot be explicitly formulated in terms of $\mathbf{U}$, direct derivation of $S_{\mathbf{u}}$ and $S_{\mathbf{uu}}$ is difficult. Consider the primitive variables $\mathbf{V} = (\rho, \boldsymbol{v}^\top, p)^\top$. Note that both S and $\mathbf{U}$ can be explicitly formulated in terms of $\mathbf{V}$; then it is easy to derive

$$\frac{\partial S}{\partial \mathbf{V}} = \left(-\Gamma/\rho,\ \mathbf{0}_d^\top,\ 1/p\right), \qquad \frac{\partial \mathbf{U}}{\partial \mathbf{V}} = \begin{pmatrix} W & \rho W^3 \boldsymbol{v}^\top & 0 \\ W^2\boldsymbol{v} & \rho h W^2 \mathbf{I}_d + 2\rho h W^4 \boldsymbol{v}\boldsymbol{v}^\top & \frac{\Gamma W^2}{\Gamma - 1}\boldsymbol{v} \\ W^2 & 2\rho h W^4 \boldsymbol{v}^\top & \frac{\Gamma W^2}{\Gamma - 1} - 1 \end{pmatrix},$$

where $\mathbf{I}_d$ denotes the identity matrix of size d. The inverse of the matrix $\frac{\partial \mathbf{U}}{\partial \mathbf{V}}$ gives

$$\frac{\partial \mathbf{V}}{\partial \mathbf{U}} = \frac{1}{\rho h(1 - c_s^2\|\boldsymbol{v}\|^2)} \begin{pmatrix} \rho h(1 - (\Gamma-1)\|\boldsymbol{v}\|^2)W^{-1} & -\rho(1 + (\Gamma-1)\|\boldsymbol{v}\|^2)\boldsymbol{v}^\top & \rho\Gamma\|\boldsymbol{v}\|^2 \\ (\Gamma-1)W^{-3}\boldsymbol{v} & \mathbf{A}_2 & \Gamma\left(\|\boldsymbol{v}\|^2 - 1\right)\boldsymbol{v} \\ -(\Gamma p + (\Gamma-1)\rho)W^{-1} & -(2\Gamma p + (\Gamma-1)\rho)\boldsymbol{v}^\top & \Gamma p\left(1 + \|\boldsymbol{v}\|^2\right) + (\Gamma-1)\rho \end{pmatrix}$$

with $\mathbf{A}_2 := \left(1 - \|\boldsymbol{v}\|^2\right)\left[\left(1 - c_s^2\|\boldsymbol{v}\|^2\right)\mathbf{I}_d + \left(\Gamma - 1 + c_s^2\right)\boldsymbol{v}\boldsymbol{v}^\top\right]$, and $c_s = \sqrt{\frac{\Gamma p}{\rho h}}$ denoting the acoustic wave speed in the RHD case ($0 < c_s < 1$). It follows that

$$S_{\mathbf{u}}^\top = \frac{\partial S}{\partial \mathbf{U}} = \frac{\partial S}{\partial \mathbf{V}}\frac{\partial \mathbf{V}}{\partial \mathbf{U}} = \frac{\Gamma - 1}{p}\left(-hW^{-1},\ -\boldsymbol{v}^\top,\ 1\right). \tag{2.4}$$

The derivative of $S_{\mathbf{u}}^\top$ with respect to $\mathbf{V}$ gives

$$S_{\mathbf{uv}} = \begin{pmatrix} \frac{\Gamma}{\rho^2}\sqrt{1 - \|\boldsymbol{v}\|^2} & \frac{\Gamma-1}{p} h W \boldsymbol{v}^\top & \frac{\Gamma-1}{p^2}\sqrt{1 - \|\boldsymbol{v}\|^2} \\ \mathbf{0}_d & -\frac{\Gamma-1}{p}\mathbf{I}_d & \frac{\Gamma-1}{p^2}\boldsymbol{v} \\ 0 & \mathbf{0}_d^\top & -\frac{\Gamma-1}{p^2} \end{pmatrix}.$$

Then we obtain

$$\begin{aligned} \mathbf{A}_1 &= \mathbf{e}_1 S_{\mathbf{u}}^\top + S_{\mathbf{u}}\mathbf{e}_1^\top + D S_{\mathbf{uv}}\frac{\partial \mathbf{V}}{\partial \mathbf{U}} + \frac{1}{\Gamma} D S_{\mathbf{u}} S_{\mathbf{u}}^\top \\ &= \frac{1 - \Gamma}{ph(h-1)(1 - c_s^2\|\boldsymbol{v}\|^2)} \begin{pmatrix} a_1 & a_2\boldsymbol{v}^\top & a_3 \\ a_2\boldsymbol{v} & \mathbf{A}_3 & a_4\boldsymbol{v} \\ a_3 & a_4\boldsymbol{v}^\top & a_5 \end{pmatrix} \end{aligned}$$

with

$$\begin{aligned} &a_1 := h(\Gamma - 1)W^{-1} > 0, \quad a_2 := (2h-1)(\Gamma - 1), \quad a_3 := -(\Gamma - 1)(h + (h-1)\|\boldsymbol{v}\|^2), \\ &\mathbf{A}_3 := \frac{(h-1)(1 - c_s^2\|\boldsymbol{v}\|^2)}{W}\mathbf{I}_d + W\Big((h-1)(1 - c_s^2\|\boldsymbol{v}\|^2) + \frac{1}{h}(\Gamma - 1)(2h-1)^2\Big)\boldsymbol{v}\boldsymbol{v}^\top, \\ &a_4 := W\left(h(1 - c_s^2\|\boldsymbol{v}\|^2) - \Gamma(2h-1)\right), \quad a_5 := W\left((h-1)(2\Gamma - 1)\|\boldsymbol{v}\|^2 + (\Gamma - 1)h\right). \end{aligned}$$

Consider the invertible matrix

$$\mathbf{P}_1 := \begin{pmatrix} 1 & \mathbf{0}_d^\top & 0 \\ -\frac{a_2}{a_1}\boldsymbol{v} & \mathbf{I}_d & \mathbf{0}_d \\ -\frac{a_3}{a_1} & \mathbf{0}_d^\top & 1 \end{pmatrix}.$$

A straightforward calculation gives

$$\mathbf{P}_1\mathbf{A}_1\mathbf{P}_1^\top = \frac{1-\Gamma}{ph(h-1)(1-c_s^2\|\boldsymbol{v}\|^2)}\begin{pmatrix} a_1 & \mathbf{0}_{d+1}^\top \\ \mathbf{0}_{d+1} & a_6\mathbf{A}_4 \end{pmatrix} \tag{2.5}$$

with $a_6 := (h-1)W\left(1-c_s^2\|\boldsymbol{v}\|^2\right) > 0$, and

$$\mathbf{A}_4 := \begin{pmatrix} (1-\|\boldsymbol{v}\|^2)\mathbf{I}_d + \boldsymbol{v}\boldsymbol{v}^\top & -\boldsymbol{v} \\ -\boldsymbol{v}^\top & \|\boldsymbol{v}\|^2 \end{pmatrix}. \tag{2.6}$$

Note that

$$\mathbf{P}_1 S_{\mathbf{u}} = \frac{\Gamma-1}{p}\Big(-hW^{-1}, 2(h-1)\boldsymbol{v}^\top, (1-h)(1+\|\boldsymbol{v}\|^2)\Big)^\top =: \frac{\Gamma-1}{p}\boldsymbol{b}_1. \tag{2.7}$$

Combining (2.3), (2.5), and (2.7) gives

$$\mathbf{P}_1\mathscr{E}_{\mathbf{uu}}\mathbf{P}_1^\top = a_7\mathcal{H}'(S)\mathbf{A}_5 + a_8\big(\mathcal{H}'(S) - \Gamma\mathcal{H}''(S)\big)\boldsymbol{b}_1\boldsymbol{b}_1^\top \tag{2.8}$$

with $a_7 := \frac{\Gamma-1}{ph(h-1)(1-c_s^2\|\boldsymbol{v}\|^2)} > 0$, $a_8 := \frac{D(\Gamma-1)^2}{p^2\Gamma} > 0$, and

$$\mathbf{A}_5 := \begin{pmatrix} a_1 & \mathbf{0}_{d+1}^\top \\ \mathbf{0}_{d+1} & a_6\mathbf{A}_4 \end{pmatrix}.$$

Let us study the property of $\mathbf{A}_4$ defined in (2.6). The matrix $(1-\|\boldsymbol{v}\|^2)\mathbf{I}_d + \boldsymbol{v}\boldsymbol{v}^\top$ is symmetric, and its eigenvalues consist of 1 and $1-\|\boldsymbol{v}\|^2$, which are both positive, implying that $(1-\|\boldsymbol{v}\|^2)\mathbf{I}_d + \boldsymbol{v}\boldsymbol{v}^\top$ is positive definite. Furthermore, a direct calculation shows $\det(\mathbf{A}_4) = 0$. Therefore, $\mathbf{A}_4$ is positive semidefinite, and $\operatorname{rank}(\mathbf{A}_4) = d$. Since $a_1 > 0$ and $a_6 > 0$, it follows that $\mathbf{A}_5$ is positive semidefinite, and $\operatorname{rank}(\mathbf{A}_5) = d+1$. Hence, there exists a rank-$(d+1)$ matrix $\mathbf{A}_6 \in \mathbb{R}^{(d+1)\times(d+2)}$ such that

$$\mathbf{A}_5 = \mathbf{A}_6^\top\mathbf{A}_6. \tag{2.9}$$

Because $\mathscr{E}_{\mathbf{uu}}$ and $\mathbf{P}_1\mathscr{E}_{\mathbf{uu}}\mathbf{P}_1^\top$ are congruent, it suffices to prove that the matrix $\mathbf{P}_1\mathscr{E}_{\mathbf{uu}}\mathbf{P}_1^\top$ is positive definite if and only if $\mathcal{H}(S)$ satisfies the condition (2.2).

(i). First, prove the condition (2.2) is sufficient for the positive definiteness of $\mathbf{P}_1\mathscr{E}_{\mathbf{uu}}\mathbf{P}_1^\top$. Because $\mathbf{A}_5$ and $\boldsymbol{b}_1\boldsymbol{b}_1^\top$ are both positive semidefinite, by (2.8) we know that $\mathbf{P}_1\mathscr{E}_{\mathbf{uu}}\mathbf{P}_1^\top$ is positive semidefinite under the condition (2.2). This means

$$\boldsymbol{z}^\top\mathbf{P}_1\mathscr{E}_{\mathbf{uu}}\mathbf{P}_1^\top\boldsymbol{z} \geq 0 \qquad \forall \boldsymbol{z} \in \mathbb{R}^{d+2}. \tag{2.10}$$

Hence, it suffices to show $\boldsymbol{z} = \mathbf{0}$ when $\boldsymbol{z}^\top\mathbf{P}_1\mathscr{E}_{\mathbf{uu}}\mathbf{P}_1^\top\boldsymbol{z} = 0$. Using (2.8) and (2.9), we obtain

$$\boldsymbol{z}^\top\mathbf{P}_1\mathscr{E}_{\mathbf{uu}}\mathbf{P}_1^\top\boldsymbol{z} = a_7\mathcal{H}'(S)\|\mathbf{A}_6\boldsymbol{z}\|^2 + a_8\big(\mathcal{H}'(S) - \Gamma\mathcal{H}''(S)\big)\left|\boldsymbol{b}_1^\top\boldsymbol{z}\right|^2 = 0,$$

which implies $\mathbf{A}_6\boldsymbol{z} = \mathbf{0}_{d+1}$ and $\boldsymbol{b}_1^\top\boldsymbol{z} = 0$. Then $\mathbf{A}_5\boldsymbol{z} = \mathbf{A}_6^\top\mathbf{A}_6\boldsymbol{z} = \mathbf{0}$. Let $\boldsymbol{z} =: (z^{(1)}, \boldsymbol{z}^{(2)}, z^{(3)})^\top$ with $\boldsymbol{z}^{(2)} \in \mathbb{R}^d$. From $\mathbf{A}_5\boldsymbol{z} = \mathbf{0}$ we can deduce that $a_1 z^{(1)} = 0$ and $a_6\mathbf{A}_4(\boldsymbol{z}^{(2)}, z^{(3)})^\top = \mathbf{0}$. This further yields $z^{(1)} = 0$ and

$$(1-\|\boldsymbol{v}\|^2)\boldsymbol{z}^{(2)} + \boldsymbol{v}\boldsymbol{v}^\top\boldsymbol{z}^{(2)} - z^{(3)}\boldsymbol{v} = \mathbf{0}_d, \tag{2.11}$$

$$-\boldsymbol{v}^\top\boldsymbol{z}^{(2)} + \|\boldsymbol{v}\|^2 z^{(3)} = 0. \tag{2.12}$$

Combining $z^{(1)}=0$ and $\boldsymbol{b}_1^\top \boldsymbol{z}=0$ gives

$$2(h-1)\boldsymbol{v}^\top \boldsymbol{z}^{(2)}+(1-h)(1+\|\boldsymbol{v}\|^2)z^{(3)}=0,$$

which, together with (2.12), implies $\boldsymbol{v}^\top \boldsymbol{z}^{(2)}=z^{(3)}=0$. Substituting it into (2.11) gives $\boldsymbol{z}^{(2)}=\mathbf{0}_d$. Therefore, we have $\boldsymbol{z}=\mathbf{0}$ when $\boldsymbol{z}^\top \mathbf{P}_1\mathscr{E}_{\mathbf{uu}}\mathbf{P}_1^\top \boldsymbol{z}=0$. This along with (2.10) yields that $\mathbf{P}_1\mathscr{E}_{\mathbf{uu}}\mathbf{P}_1^\top$ is positive definite under the condition (2.2). We complete the proof of sufficiency.

(ii). We then prove the condition (2.2) is necessary for the positive definiteness of $\mathbf{P}_1\mathscr{E}_{\mathbf{uu}}\mathbf{P}_1^\top$. Assume that $\mathbf{P}_1\mathscr{E}_{\mathbf{uu}}\mathbf{P}_1^\top$ is positive definite; then

(2.13)
$$\boldsymbol{z}^\top \mathbf{P}_1\mathscr{E}_{\mathbf{uu}}\mathbf{P}_1^\top \boldsymbol{z}=a_7\mathcal{H}'(S)\boldsymbol{z}^\top \mathbf{A}_5\boldsymbol{z}+a_8\big(\mathcal{H}'(S)-\Gamma\mathcal{H}''(S)\big)\left|\boldsymbol{b}_1^\top \boldsymbol{z}\right|^2>0\ \ \forall \boldsymbol{z}\in\mathbb{R}^{d+2}\setminus\{\mathbf{0}\}.$$

Note that the matrix $\mathbf{A}_5$ does not have full rank. There exist two vectors $\boldsymbol{z}_1,\boldsymbol{z}_2\in\mathbb{R}^{d+2}\setminus\{\mathbf{0}\}$ such that $\mathbf{A}_5\boldsymbol{z}_1=\mathbf{0}$ and $\boldsymbol{b}_1^\top \boldsymbol{z}_2=0$, respectively. It follows from (2.13) that

$$\begin{aligned}
&0<\boldsymbol{z}_2^\top \mathbf{P}_1\mathscr{E}_{\mathbf{uu}}\mathbf{P}_1^\top \boldsymbol{z}_2=a_7\mathcal{H}'(S)\boldsymbol{z}_2^\top \mathbf{A}_5\boldsymbol{z}_2=a_7\mathcal{H}'(S)\|\mathbf{A}_6\boldsymbol{z}_2\|^2,\\
&0<\boldsymbol{z}_1^\top \mathbf{P}_1\mathscr{E}_{\mathbf{uu}}\mathbf{P}_1^\top \boldsymbol{z}_1=a_8\big(\mathcal{H}'(S)-\Gamma\mathcal{H}''(S)\big)\left|\boldsymbol{b}_1^\top \boldsymbol{z}_1\right|^2,
\end{aligned}$$

which imply $\mathcal{H}'(S)>0$ and $\mathcal{H}'(S)-\Gamma\mathcal{H}''(S)>0$, respectively. The proof of necessity is complete. ∎

Remark 2.2. Proposition 2.1 and (2.1) imply that there exist a family of (generalized) entropy pairs $(\mathscr{E},\mathscr{F}_i)$ associated with the d-dimensional ($1\le d\le 3$) RHD equations (1.1),

$$\mathscr{E}(\mathbf{U})=-D\mathcal{H}(S),\qquad \mathscr{F}_i(\mathbf{U})=-Dv_i\mathcal{H}(S),\quad i=1,\dots,d, \tag{2.14}$$

generated by the smooth functions $\mathcal{H}(S)$ satisfying (2.2). Our found condition (2.2) is consistent with the one derived by Harten [12, section 2] for the two-dimensional (2D) nonrelativistic Euler system. However, the analyses in the RHD case do not directly follow from [12] but are more difficult. Due to the complicated structures of the matrix $\mathscr{E}_{\mathbf{uu}}$, some standard approaches for studying its positive definiteness, e.g., checking the positivity of its leading principal minors, can be intractable in our RHD case.

2.2. Minimum principle of the specific entropy. We are now in a position to verify that Tadmor's minimum entropy principle (1.9) also holds for the RHD system (1.1). We consider the convex entropy $\mathscr{E}(\mathbf{U})=-D\mathcal{H}(S)$ established in section 2.1 for all smooth functions $\mathcal{H}(S)$ satisfying (2.2).

Assume that $\mathbf{U}(\boldsymbol{x},t)$ is an entropy solution of the RHD equations (1.1). According to [26, Theorem 4.1] and following [27, Lemma 3.1], we have, for all smooth functions $\mathcal{H}(S)$ satisfying (2.2),

$$\int_{\|\boldsymbol{x}-\boldsymbol{x}_0\|\le R} D(\boldsymbol{x},t+\tau)\mathcal{H}(S(\boldsymbol{x},t+\tau))\mathrm{d}\boldsymbol{x}\ge \int_{\|\boldsymbol{x}-\boldsymbol{x}_0\|\le R+\tau v_{\max}} D(\boldsymbol{x},t)\mathcal{H}(S(\boldsymbol{x},t))\mathrm{d}\boldsymbol{x}\qquad \forall R>0,$$

where $v_{\max}$ denotes the maximal wave speed in the domain; we can take $v_{\max}$ as the speed of light $c=1$, a simple upper bound of all wave speeds in the RHD case. Note that the density involved in (2.15) is $D=\rho W$ instead of the rest-mass density ρ.

Consider a special function $\mathcal{H}_0(S)$ [27] defined by

$$\mathcal{H}_0(S) := \min\{S - S_0, 0\}, \qquad S_0 = \min\left\{S(\boldsymbol{y}, t) : \ \|\boldsymbol{y} - \boldsymbol{x}_0\| \le R + \tau v_{\max}\right\}.$$

As observed in [27], the function $\mathcal{H}_0(S)$, although not smooth, can be written as the limit of a sequence of smooth functions satisfying (2.2); see also [5, section 3.1] for a detailed review. Therefore, by passing to the limit, the inequality (2.15) holds for $\mathcal{H} = \mathcal{H}_0$, which gives

$$\int_{\|\boldsymbol{x}-\boldsymbol{x}_0\|\le R} D(\boldsymbol{x}, t+\tau)\min\{S(\boldsymbol{x}, t+\tau) - S_0, 0\}\mathrm{d}\boldsymbol{x} \\ \ge \int_{\|\boldsymbol{x}-\boldsymbol{x}_0\|\le R+\tau v_{\max}} D(\boldsymbol{x}, t)\mathcal{H}_0(S(\boldsymbol{x}, t))\mathrm{d}\boldsymbol{x} = 0.$$

Because $D(\boldsymbol{x}, t+\tau) > 0$, we obtain $\min\{S(\boldsymbol{x}, t+\tau) - S_0, 0\} = 0$ for $\|\boldsymbol{x} - \boldsymbol{x}_0\| \le R$. This leads to

$$S(\boldsymbol{x}, t+\tau) \ge S_0 = \min\left\{S(\boldsymbol{y}, t) : \ \|\boldsymbol{y} - \boldsymbol{x}_0\| \le R + \tau v_{\max}\right\} \qquad \forall \|\boldsymbol{x}-\boldsymbol{x}_0\| \le R, \tag{2.15}$$

which yields the local minimum entropy principle (1.9). In particular, this implies that the spatial minimum of the specific entropy, $\min_{\boldsymbol{x}} S(\boldsymbol{x}, t)$, is a nondecreasing function of time t, yielding

$$S(\boldsymbol{x}, t) \ge \min_{\boldsymbol{x}} S(\boldsymbol{x}, 0) \qquad \forall t \ge 0. \tag{2.16}$$

In the above derivation it is implicitly assumed that $\mathbf{U}(\boldsymbol{x}, t)$ always satisfies the physical constraints (1.5). The entropy principle (2.16) and the constraints (1.5) constitute the global invariant region Ω_{S_0}, defined in (1.10), for entropy solutions of the RHD equations (1.1).

3. Auxiliary theories for numerical analysis. In order to analyze the local minimum entropy principle of numerical schemes, we introduce a (more general) "local" invariant region for an arbitrarily given σ:

$$\Omega_\sigma := \left\{\mathbf{U} = (D, \boldsymbol{m}^\top, E)^\top \in \mathbb{R}^{d+2} : \ \rho(\mathbf{U}) > 0, \ p(\mathbf{U}) > 0, \ \|\boldsymbol{v}(\mathbf{U})\| < 1, \ S(\mathbf{U}) \ge \sigma\right\}. \tag{3.1}$$

The special choice $\sigma = S_0 = \operatorname{ess\,inf}_{\boldsymbol{x}} S(\boldsymbol{x}, 0)$ corresponds to the global invariant region Ω_{S_0} in (1.10). It is evident that the following "monotonicity" holds for Ω_σ.

LEMMA 3.1 (monotonic decreasing). *If $\sigma_1 \ge \sigma_2$, then $\Omega_{\sigma_1} \subseteq \Omega_{\sigma_2}$.*

Thanks to $\mathcal{G} = \mathcal{G}_1$ proved in [34, Lemma 2.1], we immediately have the following lemma.

LEMMA 3.2 (first equivalent form). *The invariant region set Ω_σ is equivalent to*

$$\Omega_\sigma^{(1)} = \left\{\mathbf{U} = (D, \boldsymbol{m}^\top, E)^\top \in \mathbb{R}^{d+2} : \ D > 0, \ E > \sqrt{D^2 + \|\boldsymbol{m}\|^2}, \ S(\mathbf{U}) \ge \sigma\right\}. \tag{3.2}$$

The specific entropy $S = \log(p\rho^{-\Gamma})$ is a nonlinear function of (ρ, p), and, as mentioned in section 1, the functions $\rho(\mathbf{U})$ and $p(\mathbf{U})$ are already nonlinear and without explicit formulas. The combination of these nonlinear functions leads to $S(\mathbf{U})$, which is a highly nonlinear function and also cannot be explicitly formulated in terms of $\mathbf{U}$. This makes it difficult to study the minimum entropy principle at the numerical level and explore IRP schemes for RHD. In order to overcome these challenges, several important properties of the invariant region Ω_σ will be derived in this section.

3.1. An explicit and linear equivalent form of invariant region. To address the difficulties arising from the nonlinearity of $S(\mathbf{U})$, we discover the following novel equivalent form of Ω_σ.

THEOREM 3.3 (second equivalent form). *The invariant region set Ω_σ is equivalent to*

$$\Omega_\sigma^{(2)} = \big\{\mathbf{U} = (D, \boldsymbol{m}^\top, E)^\top \in \mathbb{R}^{d+2} : \ D > 0, \\ \varphi_\sigma(\mathbf{U}; \boldsymbol{v}_*, \rho_*) \geq 0 \ \forall \boldsymbol{v}_* \in \mathbb{B}_1(\mathbf{0}), \ \forall \rho_* \in \mathbb{R}^+\big\}, \tag{3.3}$$

where $\mathbb{B}_1(\mathbf{0}) := \{\boldsymbol{x} \in \mathbb{R}^d : |\boldsymbol{x}| < 1\}$ denotes the open unit ball centered at $\mathbf{0}$ in $\mathbb{R}^d$, and

$$\varphi_\sigma(\mathbf{U}; \boldsymbol{v}_*, \rho_*) := E - \boldsymbol{m}\cdot\boldsymbol{v}_* - D\sqrt{1-\|\boldsymbol{v}_*\|^2} + \mathrm{e}^\sigma\left(\rho_*^\Gamma - \frac{\Gamma}{\Gamma-1} D\rho_*^{\Gamma-1}\sqrt{1-\|\boldsymbol{v}_*\|^2}\right). \tag{3.4}$$

Before proving Theorem 3.3, we mention a crucial feature of the above equivalent form $\Omega_\sigma^{(2)}$. Note that all the "nonlinear" constraints in $\Omega_\sigma^{(1)}$ or Ω_σ are *equivalently* transformed into a *linear* constraint $\varphi_\sigma(\mathbf{U}; \boldsymbol{v}_*, \rho_*) \geq 0$ in (3.3). As a result, all the constraints in $\Omega_\sigma^{(2)}$ are *explicit* and *linear* with respect to $\mathbf{U}$, although two (additional) auxiliary variables $\boldsymbol{v}_*$ and ρ_* are introduced here. Such linearity makes $\Omega_\sigma^{(2)}$ very useful for analytically verifying the IRP property of RHD schemes. This becomes a key to our IRP analysis, which is significantly different from the standard bound-preserving and IRP analysis techniques in, e.g., [41, 42, 16].

We first give two useful lemmas, whose proofs can be found in sections SM2 and SM3 of the supplementary material.

LEMMA 3.4. *For any $\eta > -\frac{1}{2}$, we have $(\eta\Gamma+1)^{\frac{1}{\Gamma}} \geq (2\eta+1)^{\frac{1}{2}}$, where the adiabatic index $\Gamma \in (1, 2]$.*

LEMMA 3.5. *For any $\boldsymbol{v}, \boldsymbol{v}_* \in \mathbb{B}_1(\mathbf{0})$, it holds that*

$$\frac{\Gamma(1-\boldsymbol{v}\cdot\boldsymbol{v}_*)}{1-\|\boldsymbol{v}\|^2} - \Gamma + 1 \geq \left(\frac{\sqrt{1-\|\boldsymbol{v}\|^2}}{\sqrt{1-\|\boldsymbol{v}_*\|^2}}\right)^{-\Gamma}. \tag{3.5}$$

We are now in a position to prove Theorem 3.3.

Proof of Theorem 3.3. The proof of $\Omega_\sigma = \Omega_\sigma^{(2)}$ consists of showing that $\Omega_\sigma^{(2)} \subseteq \Omega_\sigma$ and that $\Omega_\sigma \subseteq \Omega_\sigma^{(2)}$.

(i). Prove that $\mathbf{U} \in \Omega_\sigma^{(2)} \Rightarrow \mathbf{U} \in \Omega_\sigma$. When $\mathbf{U} = (D, \boldsymbol{m}^\top, E)^\top \in \Omega_\sigma^{(2)}$, by definition we have $D > 0$ and

$$\varphi_\sigma(\mathbf{U}; \boldsymbol{v}_*, \rho_*) \geq 0 \qquad \forall \boldsymbol{v}_* \in \mathbb{B}_1(\mathbf{0}), \quad \forall \rho_* \in \mathbb{R}^+. \tag{3.6}$$

If we take a special $(\boldsymbol{v}_*, \rho_*) = \big(\frac{\boldsymbol{m}}{\sqrt{D^2+\|\boldsymbol{m}\|^2}}, \frac{D^2}{\sqrt{D^2+\|\boldsymbol{m}\|^2}}\big)$, which satisfies $\boldsymbol{v}_* \in \mathbb{B}_1(\mathbf{0})$ and $\rho_* > 0$, then

$$\begin{aligned} 0 &\leq \varphi_\sigma\left(\mathbf{U}; \frac{\boldsymbol{m}}{\sqrt{D^2+\|\boldsymbol{m}\|^2}}, \frac{D^2}{\sqrt{D^2+\|\boldsymbol{m}\|^2}}\right) \\ &= E - \sqrt{D^2+\|\boldsymbol{m}\|^2} - \frac{\mathrm{e}^\sigma}{\Gamma-1}\left(\frac{D^2}{\sqrt{D^2+\|\boldsymbol{m}\|^2}}\right)^\Gamma < E - \sqrt{D^2+\|\boldsymbol{m}\|^2}, \end{aligned}$$

which implies the second constraint in $\mathcal{G}_1$. This, along with $D>0$, yields $\mathbf{U}\in\mathcal{G}_1=\mathcal{G}$. Therefore, the corresponding primitive quantities of $\mathbf{U}$ satisfy

$$\rho(\mathbf{U})>0,\quad p(\mathbf{U})>0,\quad \|\boldsymbol{v}(\mathbf{U})\|<1. \tag{3.7}$$

Taking another special $(\boldsymbol{v}_*,\rho_*)=(\boldsymbol{v}(\mathbf{U}),\rho(\mathbf{U}))$ in (3.6) gives

$$\begin{aligned}0&\le\varphi_\sigma\left(\mathbf{U};\boldsymbol{v}(\mathbf{U}),\rho(\mathbf{U})\right)\\&=E-\boldsymbol{m}\cdot\boldsymbol{v}-D\sqrt{1-\|\boldsymbol{v}\|^2}+\mathrm{e}^\sigma\left(\rho^\Gamma-\frac{\Gamma}{\Gamma-1}D\rho^{\Gamma-1}\sqrt{1-\|\boldsymbol{v}\|^2}\right)=\frac{p-\mathrm{e}^\sigma\rho^\Gamma}{\Gamma-1},\end{aligned}$$

which, together with $\Gamma>1$, imply $p\ge\mathrm{e}^\sigma\rho^\Gamma$. It follows that $S(\mathbf{U})=\log(p\rho^{-\Gamma})\ge\sigma$. Combining it with (3.7), we obtain $\mathbf{U}\in\Omega_\sigma$.

(ii). We prove that $\mathbf{U}\in\Omega_\sigma\Rightarrow\mathbf{U}\in\Omega_\sigma^{(2)}$. When $\mathbf{U}=(D,\boldsymbol{m}^\top,E)^\top\in\Omega_\sigma$, the corresponding primitive quantities satisfy

$$\rho>0,\quad \|\boldsymbol{v}\|<1,\quad p\ge\mathrm{e}^\sigma\rho^\Gamma. \tag{3.8}$$

This immediately gives $D=\rho W=\rho\left(1-\|\boldsymbol{v}\|^2\right)^{-\frac{1}{2}}>0$. It remains to prove $\varphi_\sigma(\mathbf{U};\boldsymbol{v}_*,\rho_*)\ge0$ for any $\boldsymbol{v}_*\in\mathbb{B}_1(\mathbf{0})$ and any $\rho_*>0$. Let us rewrite $\varphi_\sigma(\mathbf{U};\boldsymbol{v}_*,\rho_*)$ as

$$\varphi_\sigma(\mathbf{U};\boldsymbol{v}_*,\rho_*)=\Pi_1p+\Pi_2,$$

with

$$\begin{aligned}\Pi_1&:=\frac{\Gamma}{\Gamma-1}\left(\frac{1-\boldsymbol{v}\cdot\boldsymbol{v}_*}{1-\|\boldsymbol{v}\|^2}\right)-1\ge2\left(\frac{1-\boldsymbol{v}\cdot\boldsymbol{v}_*}{1-\|\boldsymbol{v}\|^2}\right)-1=\frac{(1-\|\boldsymbol{v}\|)^2+2\left(\|\boldsymbol{v}\|-\boldsymbol{v}\cdot\boldsymbol{v}_*\right)}{1-\|\boldsymbol{v}\|^2}\\&>0,\\\Pi_2&:=\rho\left(\frac{1-\boldsymbol{v}\cdot\boldsymbol{v}_*}{1-\|\boldsymbol{v}\|^2}-\frac{\sqrt{1-\|\boldsymbol{v}_*\|^2}}{\sqrt{1-\|\boldsymbol{v}\|^2}}\right)+\mathrm{e}^\sigma\left(\rho_*^\Gamma-\frac{\Gamma}{\Gamma-1}\rho\rho_*^{\Gamma-1}\frac{\sqrt{1-\|\boldsymbol{v}_*\|^2}}{\sqrt{1-\|\boldsymbol{v}\|^2}}\right),\end{aligned}$$

where $\Gamma\in(1,2]$ and $\|\boldsymbol{v}\|<1$ are used in showing $\Pi_1>0$. Then, using $p\ge\mathrm{e}^\sigma\rho^\Gamma$ gives

$$\begin{aligned}\varphi_\sigma(\mathbf{U};\boldsymbol{v}_*,\rho_*)&\ge\Pi_1\mathrm{e}^\sigma\rho^\Gamma+\Pi_2=\frac{\rho}{1-\|\boldsymbol{v}\|^2}\left(1-\boldsymbol{v}\cdot\boldsymbol{v}_*-\sqrt{1-\|\boldsymbol{v}\|^2}\sqrt{1-\|\boldsymbol{v}_*\|^2}\right)\\&\quad+\mathrm{e}^\sigma\rho^\Gamma\Pi_3\\&\ge\frac{\rho}{1-\|\boldsymbol{v}\|^2}\left(1-\sqrt{\|\boldsymbol{v}\|^2+(1-\|\boldsymbol{v}\|^2)}\sqrt{\|\boldsymbol{v}_*\|^2+(1-\|\boldsymbol{v}_*\|^2)}\right)+\mathrm{e}^\sigma\rho^\Gamma\Pi_3\\&=\mathrm{e}^\sigma\rho^\Gamma\Pi_3,\end{aligned} \tag{3.9}$$

where the Cauchy–Schwarz inequality has been used, and $\Pi_3:=\phi_\sigma\left(\frac{\rho}{\rho_*};\boldsymbol{v},\boldsymbol{v}_*\right)$ with

$$\phi_\sigma(x;\boldsymbol{v},\boldsymbol{v}_*):=x^{-\Gamma}-\frac{\Gamma\sqrt{1-\|\boldsymbol{v}_*\|^2}}{(\Gamma-1)\sqrt{1-\|\boldsymbol{v}\|^2}}x^{-\Gamma+1}+\frac{\Gamma(1-\boldsymbol{v}\cdot\boldsymbol{v}_*)}{(\Gamma-1)\left(1-\|\boldsymbol{v}\|^2\right)}-1,\quad x>0.$$

It is easy to verify that the function $\phi_\sigma(x;\boldsymbol{v},\boldsymbol{v}_*)$ is strictly decreasing on the interval $\left(0,\frac{\sqrt{1-\|\boldsymbol{v}\|^2}}{\sqrt{1-\|\boldsymbol{v}_*\|^2}}\right]$ and strictly increasing on $\left[\frac{\sqrt{1-\|\boldsymbol{v}\|^2}}{\sqrt{1-\|\boldsymbol{v}_*\|^2}},+\infty\right)$ with respect to x. Therefore, we have

$$\Pi_3\ge\min_{x\in\mathbb{R}^+}\phi_\sigma(x;\boldsymbol{v},\boldsymbol{v}_*)=\phi_\sigma\left(\frac{\sqrt{1-\|\boldsymbol{v}\|^2}}{\sqrt{1-\|\boldsymbol{v}_*\|^2}};\boldsymbol{v},\boldsymbol{v}_*\right)$$

$$= \frac{1}{\Gamma-1}\left[-\left(\frac{\sqrt{1-\|\boldsymbol{v}\|^2}}{\sqrt{1-\|\boldsymbol{v}_*\|^2}}\right)^{-\Gamma} + \frac{\Gamma(1-\boldsymbol{v}\cdot\boldsymbol{v}_*)}{1-\|\boldsymbol{v}\|^2} - \Gamma + 1\right] \geq 0, \tag{3.10}$$

where we used $\Gamma \in (1,2]$ and inequality (3.5) in Lemma 3.5. Then combining (3.1)–(3.10), we conclude $\varphi_\sigma(\mathbf{U};\boldsymbol{v}_*,\rho_*) \geq \mathrm{e}^\sigma \rho^\Gamma \Pi_3 \geq 0$. This, along with $D>0$, implies $\mathbf{U} \in \Omega_\sigma^{(2)}$. The proof is now complete. ∎

Considering $\sigma \to -\infty$ in Ω_σ and using Theorem 3.3, one can also obtain the following corollary.

COROLLARY 3.6. *The admissible state set $\mathcal{G}$ is equivalent to*

$$\begin{aligned}\mathcal{G}_2 := \big\{\mathbf{U} = (D, \boldsymbol{m}^\top, E)^\top \in \mathbb{R}^{d+2} :\ & D>0,\\ & E > \boldsymbol{m}\cdot\boldsymbol{v}_* + D\sqrt{1-\|\boldsymbol{v}_*\|^2}\ \forall \boldsymbol{v}_* \in \mathbb{B}_1(\mathbf{0})\big\}.\end{aligned}$$

3.2. Convexity of invariant region. The convexity of an invariant region is a highly desirable property, as it can be used to simplify the IRP analysis of those numerical schemes that can be reformulated into some suitable convex combinations; see, for example, [41, 42, 29, 16]. For the RHD case, the convexity of the invariant region Ω_σ is discussed below.

LEMMA 3.7. *For any fixed $\sigma \in \mathbb{R}$, the invariant region Ω_σ is a convex set.*

Proof. Since $\Omega_\sigma = \Omega_\sigma^{(2)}$, one need only show the convexity of $\Omega_\sigma^{(2)}$. For any $\mathbf{U}_1 = (D_1, \boldsymbol{m}_1^\top, E_1)^\top$, $\mathbf{U}_2 = (D_2, \boldsymbol{m}_2^\top, E_2)^\top \in \Omega_\sigma^{(2)}$, and any $\lambda \in [0,1]$, we have $\lambda D_1 + (1-\lambda)D_2 > 0$, and for any $\boldsymbol{v}_* \in \mathbb{B}_1(\mathbf{0})$, $\rho_* \in \mathbb{R}^+$, it holds that

$$\varphi_\sigma\big(\lambda\mathbf{U}_1 + (1-\lambda)\mathbf{U}_2; \boldsymbol{v}_*, \rho_*\big) = \lambda\varphi_\sigma(\mathbf{U}_1;\boldsymbol{v}_*,\rho_*) + (1-\lambda)\varphi_\sigma(\mathbf{U}_2;\boldsymbol{v}_*,\rho_*) \geq 0,$$

where the linearity of $\varphi_\sigma(\mathbf{U};\boldsymbol{v}_*,\rho_*)$ with respect to $\mathbf{U}$ has been used. Hence, we obtain $\lambda\mathbf{U}_1 + (1-\lambda)\mathbf{U}_2 \in \Omega_\sigma^{(2)}$, and by definition, $\Omega_\sigma^{(2)}$ is a convex set. ∎

The following more general conclusion can be shown by using Lemmas 3.7 and 3.1.

LEMMA 3.8. *Let σ_1 and σ_2 be two real numbers. For any $\mathbf{U}_1 \in \Omega_{\sigma_1}$ and any $\mathbf{U}_2 \in \Omega_{\sigma_2}$,*

$$\lambda\mathbf{U}_1 + (1-\lambda)\mathbf{U}_2 \in \Omega_{\min\{\sigma_1,\sigma_2\}} \qquad \forall \lambda \in [0,1].$$

Proof. With the help of Lemma 3.1, we have $\mathbf{U}_i \in \Omega_{\sigma_i} \subseteq \Omega_{\min\{\sigma_1,\sigma_2\}}$, $i=1,2$. The proof is then completed by using the convexity of $\Omega_{\min\{\sigma_1,\sigma_2\}}$. ∎

An alternative proof based on Jensen's inequality is also provided in section SM4 of the supplementary material.

3.3. Generalized Lax–Friedrichs splitting properties. In the bound-preserving analysis of numerical schemes with the LF flux, the following property (3.11) is usually expected:

$$\mathbf{U} \pm \frac{\mathbf{F}_i(\mathbf{U})}{\alpha} \in \Omega_\sigma \quad \forall \mathbf{U} \in \Omega_\sigma,\ \forall \alpha \geq \alpha_i, \tag{3.11}$$

where α_i denotes an appropriate upper bound for the wave speeds in the x_i-direction; for the RHD system it can be taken as the speed of light. We refer to (3.11) as the

LF splitting property. This property is valid for the admissible state set $\mathcal{G}$ or $\mathcal{G}_1$ and played an important role in constructing bound-preserving schemes for the RHD; see [34, 24, 37]. Unfortunately, however, the property (3.11) does *not* hold in general for the invariant region Ω_σ as the entropy principle $S(\mathbf{U}) \geq \sigma$ is included.

Since (3.11) is invalid for Ω_σ, we look for some alternative properties that hold for Ω_σ but are weaker than (3.11). This motivates us to study a suitable convex combination of several different terms like $\mathbf{U} \pm \frac{\mathbf{F}_i(\mathbf{U})}{\alpha}$, so that we finally achieve *generalized LF (gLF) splitting properties*, whose derivations are highly nontrivial. Built on a technical inequality (3.12) constructed in section 3.3.1, the gLF splitting properties are presented in section 3.3.2.

3.3.1. A constructive inequality. An important inequality (3.12) is first constructed, which will be the key to establishing the gLF splitting properties.

THEOREM 3.9. *If* $\mathbf{U} \in \Omega_\sigma$*, then for any* $\boldsymbol{v}_* = (v_{1,*}, \ldots, v_{d,*})^\top \in \mathbb{B}_1(\mathbf{0})$*, any* $\rho_* \in \mathbb{R}^+$*, and any* $\theta \in [-1, 1]$*, it holds that*

$$\varphi_\sigma\Big(\mathbf{U} + \theta \mathbf{F}_i(\mathbf{U}); \boldsymbol{v}_*, \rho_*\Big) + \theta \mathrm{e}^\sigma v_{i,*} \rho_*^\Gamma \geq 0, \tag{3.12}$$

where $i \in \{1, \ldots, d\}$*, and the function* φ_σ *is defined in* (3.4).

Proof. Due to the relativistic effects, the flux $\mathbf{F}_i(\mathbf{U})$ also cannot be explicitly formulated in terms of $\mathbf{U}$. Therefore, we have to work on the corresponding primitive quantities $\{\rho, \boldsymbol{v}, p\}$ of $\mathbf{U}$, which satisfy $\rho > 0$, $\|\boldsymbol{v}\| < 1$, and $p \geq \mathrm{e}^\sigma \rho^\Gamma$ because $\mathbf{U} \in \Omega_\sigma$. We observe that

$$\varphi_\sigma\Big(\mathbf{U} + \theta \mathbf{F}_i(\mathbf{U}); \boldsymbol{v}_*, \rho_*\Big) + \theta \mathrm{e}^\sigma v_{i,*} \rho_*^\Gamma = \widehat{\Pi}_1 + \widehat{\Pi}_2 p + \mathrm{e}^\sigma \widehat{\Pi}_3,$$

with

$$\begin{aligned}
\widehat{\Pi}_1 &:= \rho W^2 (1 + \theta v_i) \left(1 - \boldsymbol{v} \cdot \boldsymbol{v}_* - \sqrt{1 - \|\boldsymbol{v}\|^2} \sqrt{1 - \|\boldsymbol{v}_*\|^2}\right), \\
\widehat{\Pi}_2 &:= \frac{\Gamma}{\Gamma - 1} (1 + \theta v_i) \left(\frac{1 - \boldsymbol{v} \cdot \boldsymbol{v}_*}{1 - \|\boldsymbol{v}\|^2}\right) - (1 + \theta v_{i,*}), \\
\widehat{\Pi}_3 &:= \rho_*^\Gamma (1 + \theta v_{i,*}) - \frac{\Gamma}{\Gamma - 1} (1 + \theta v_i) \rho W \rho_*^{\Gamma - 1} \sqrt{1 - \|\boldsymbol{v}_*\|^2}.
\end{aligned}$$

Using the Cauchy–Schwarz inequality gives

$$\boldsymbol{v} \cdot \boldsymbol{v}_* + \sqrt{1 - \|\boldsymbol{v}\|^2} \sqrt{1 - \|\boldsymbol{v}_*\|^2} \leq \sqrt{\|\boldsymbol{v}\|^2 + (1 - \|\boldsymbol{v}\|^2)} \sqrt{\|\boldsymbol{v}_*\|^2 + (1 - \|\boldsymbol{v}_*\|^2)} = 1,$$

which implies $\widehat{\Pi}_1 \geq 0$. It follows that

$$\varphi_\sigma\Big(\mathbf{U} + \theta \mathbf{F}_i(\mathbf{U}); \boldsymbol{v}_*, \rho_*\Big) + \theta \mathrm{e}^\sigma v_{i,*} \rho_*^\Gamma \geq \widehat{\Pi}_2 p + \mathrm{e}^\sigma \widehat{\Pi}_3. \tag{3.13}$$

Recalling that $\Gamma \in (1, 2]$, $\|\boldsymbol{v}\| < 1$, and $\|\boldsymbol{v}_*\| < 1$, we obtain

$$\widehat{\Pi}_2 \geq 2 \left(\frac{1 + \theta v_i}{1 - \|\boldsymbol{v}\|^2}\right) (1 - \boldsymbol{v} \cdot \boldsymbol{v}_*) - (1 + \theta v_{i,*}) =: \widetilde{\Pi}_2 > 0, \tag{3.14}$$

where the positivity of $\widetilde{\Pi}_2$ is deduced by using the Cauchy–Schwarz inequality as

follows:

$$\begin{aligned}
\widetilde{\Pi}_2 &= 2\left(\frac{1+\theta v_i}{1-\|\boldsymbol{v}\|^2}\right) - 1 - 2\left(\frac{1+\theta v_i}{1-\|\boldsymbol{v}\|^2}\right)\left[\left(v_i + \frac{\theta(1-\|\boldsymbol{v}\|^2)}{2(1+\theta v_i)}\right) v_{i,*} + \sum_{j\neq i} v_j v_{j,*}\right] \\
&\geq 2\left(\frac{1+\theta v_i}{1-\|\boldsymbol{v}\|^2}\right) - 1 - 2\left(\frac{1+\theta v_i}{1-\|\boldsymbol{v}\|^2}\right)\left[\left(v_i + \frac{\theta(1-\|\boldsymbol{v}\|^2)}{2(1+\theta v_i)}\right)^2 + \sum_{j\neq i} v_j^2\right]^{\frac{1}{2}} \|\boldsymbol{v}_*\| \\
&= 2\left(\frac{1+\theta v_i}{1-\|\boldsymbol{v}\|^2}\right) - 1 - 2\left(\frac{1+\theta v_i}{1-\|\boldsymbol{v}\|^2}\right)\|\boldsymbol{v}_*\|\left[1 - \frac{1-\|\boldsymbol{v}\|^2}{1+\theta v_i} + \frac{\theta^2(1-\|\boldsymbol{v}\|^2)^2}{4(1+\theta v_i)^2}\right]^{\frac{1}{2}} \\
&\geq 2\left(\frac{1+\theta v_i}{1-\|\boldsymbol{v}\|^2}\right) - 1 - 2\left(\frac{1+\theta v_i}{1-\|\boldsymbol{v}\|^2}\right)\|\boldsymbol{v}_*\|\left[\left(1 - \frac{1-\|\boldsymbol{v}\|^2}{2(1+\theta v_i)}\right)^2\right]^{\frac{1}{2}} \\
&= \left[2\left(\frac{1+\theta v_i}{1-\|\boldsymbol{v}\|^2}\right) - 1\right](1-\|\boldsymbol{v}_*\|) \geq \left[2\left(\frac{1-\|\boldsymbol{v}\|}{1-\|\boldsymbol{v}\|^2}\right) - 1\right](1-\|\boldsymbol{v}_*\|) > 0.
\end{aligned} \tag{3.15}$$

Combining $\widehat{\Pi}_2 > 0$ and $p \geq \mathrm{e}^{\sigma}\rho^{\Gamma}$, we then derive from (3.13) that

$$\varphi_\sigma\Big(\mathbf{U} + \theta\mathbf{F}_i(\mathbf{U}); \boldsymbol{v}_*, \rho_*\Big) + \theta\mathrm{e}^{\sigma} v_{i,*}\rho_*^{\Gamma} \geq \widehat{\Pi}_2 \mathrm{e}^{\sigma}\rho^{\Gamma} + \mathrm{e}^{\sigma}\widehat{\Pi}_3 = \mathrm{e}^{\sigma}\rho^{\Gamma}\widehat{\Pi}_4, \tag{3.16}$$

with $\widehat{\Pi}_4 := \widehat{\Pi}_2 + \rho^{-\Gamma}\widehat{\Pi}_3 = \hat{\phi}_\sigma\big(\frac{\rho}{\rho_*}; \boldsymbol{v}, \boldsymbol{v}_*\big)$ and

$$\hat{\phi}_\sigma(x; \boldsymbol{v}, \boldsymbol{v}_*) := \widehat{\Pi}_2 + x^{-\Gamma}\left(1 + \theta v_{i,*}\right) - x^{-\Gamma+1}\left(\frac{\Gamma}{\Gamma-1}(1+\theta v_i)\frac{\sqrt{1-\|\boldsymbol{v}_*\|^2}}{\sqrt{1-\|\boldsymbol{v}\|^2}}\right).$$

The subsequent task is to show that $\widehat{\Pi}_4$ is always nonnegative. Define

$$\eta_s := \frac{1+\theta v_i}{1+\theta v_{i,*}}\left(\frac{1-\boldsymbol{v}\cdot\boldsymbol{v}_*}{1-\|\boldsymbol{v}\|^2}\right) - 1, \qquad x_s := \frac{(1+\theta v_{i,*})\sqrt{1-\|\boldsymbol{v}\|^2}}{(1+\theta v_i)\sqrt{1-\|\boldsymbol{v}_*\|^2}}.$$

By studying the derivative of $\hat{\phi}_\sigma$ with respect to x, we observe that the function $\hat{\phi}_\sigma$ is strictly decreasing on the interval $(0, x_s]$ and strictly increasing on $[x_s, +\infty)$. We therefore have

$$\begin{aligned}
\widehat{\Pi}_4 &\geq \min_{x\in\mathbb{R}^+} \hat{\phi}_\sigma(x; \boldsymbol{v}, \boldsymbol{v}_*) = \hat{\phi}_\sigma(x_s; \boldsymbol{v}, \boldsymbol{v}_*) \\
&= \widehat{\Pi}_2 - \frac{1}{\Gamma-1}x_s^{-\Gamma}\left(1+\theta v_{i,*}\right) = \frac{1+\theta v_{i,*}}{\Gamma-1}\Big(\eta_s\Gamma + 1 - x_s^{-\Gamma}\Big).
\end{aligned} \tag{3.17}$$

Using the formulation of $\widetilde{\Pi}_2$ defined in (3.14), we reformulate η_s and observe that

$$\eta_s = \frac{1}{2}\left(\frac{\widetilde{\Pi}_2}{1+\theta v_{i,*}} + 1\right) - 1 = \frac{\widetilde{\Pi}_2}{2(1+\theta v_{i,*})} - \frac{1}{2} > -\frac{1}{2},$$

where the last step follows from the positivity of $\widetilde{\Pi}_2$, which has been proven in (3.15). Thanks to Lemma 3.4, we obtain $(\eta_s\Gamma+1)^{1/\Gamma} \geq (2\eta_s+1)^{1/2}$, or equivalently, $\eta_s\Gamma+1 \geq (2\eta_s+1)^{\frac{\Gamma}{2}}$, which, along with (3.17), imply

$$\widehat{\Pi}_4 \geq \frac{1+\theta v_{i,*}}{\Gamma-1}\left[\big(2\eta_s+1\big)^{\frac{\Gamma}{2}} - \big(x_s^{-2}\big)^{\frac{\Gamma}{2}}\right]. \tag{3.18}$$

Next, we would like to show that $2\eta_s+1 \geq x_s^{-2}$. Define $a_1 := \theta v_i$, $a_2 := \sqrt{\|\boldsymbol{v}\|^2 - \theta^2 v_i^2}$, $b_1 := \theta v_{i,*}$, and $b_2 := \sqrt{\|\boldsymbol{v}_*\|^2 - \theta^2 v_{i,*}^2}$. By an elementary inequality[2]

$$(1+a_1)^2(1-b_1^2-b_2^2) + (1+b_1)^2(1-a_1^2-a_2^2) \leq 2(1-a_1b_1-a_2b_2)(1+a_1)(1+b_1),$$

we get

$$x_s^{-2} = \frac{(1+a_1)^2(1-b_1^2-b_2^2)}{(1+b_1)^2(1-a_1^2-a_2^2)} \leq 2\frac{(1-a_1b_1-a_2b_2)(1+a_1)}{(1+b_1)(1-a_1^2-a_2^2)} - 1 = 2\widetilde{\eta}_s + 1 \tag{3.19}$$

with $\widetilde{\eta}_s := \frac{1+\theta v_i}{1+\theta v_{i,*}}\big(\frac{1-a_1b_1-a_2b_2}{1-\|\boldsymbol{v}\|^2}\big) - 1$. With the aid of the Cauchy–Schwarz inequality, we obtain

$$\begin{aligned}
\boldsymbol{v}\cdot\boldsymbol{v}_* &= \theta^2 v_i v_{i,*} + \Big(v_i\sqrt{1-\theta^2}\Big)\Big(v_{i,*}\sqrt{1-\theta^2}\Big) + \sum_{j\neq i} v_j v_{j,*} \\
&\leq \theta^2 v_i v_{i,*} + \left(\Big(v_i\sqrt{1-\theta^2}\Big)^2 + \sum_{j\neq i} v_j^2\right)^{\frac{1}{2}} \left(\Big(v_{i,*}\sqrt{1-\theta^2}\Big)^2 + \sum_{j\neq i} v_{j,*}^2\right)^{\frac{1}{2}} \\
&= a_1b_1 + a_2b_2,
\end{aligned}$$

which implies $\eta_s \geq \widetilde{\eta}_s$. It then follows from (3.19) that $x_s^{-2} \leq 2\eta_s + 1$, which together with (3.18) implies $\widehat{\Pi}_4 \geq 0$. Then by using (3.16), we conclude $\varphi_\sigma\big(\mathbf{U} + \theta\mathbf{F}_i(\mathbf{U}); \boldsymbol{v}_*, \rho_*\big) + \theta \mathrm{e}^\sigma v_{i,*}\rho_*^\Gamma \geq \mathrm{e}^\sigma \rho^\Gamma \widehat{\Pi}_4 \geq 0$. Hence, the inequality (3.12) holds, which completes the proof. ∎

Remark 3.10. We would like to highlight the term $(\theta \mathrm{e}^\sigma v_{i,*}\rho_*^\Gamma)$ in the inequality (3.12). It appears that this term is superfluous, as the second constraint in the equivalent form $\Omega_\sigma^{(2)}$ does not contain such a term. But in fact, this technical term is necessary and very crucial. If it is removed from (3.12), the resulting inequality would not hold any longer. Although its value is not always positive, this term helps to offset the "negative part" of $\varphi_\sigma(\mathbf{U} + \theta\mathbf{F}_i(\mathbf{U}); \boldsymbol{v}_*, \rho_*)$. Moreover, this extra term will be canceled out in our IRP analyses; see the proofs of Theorems 3.11–3.13.

3.3.2. Derivation of gLF splitting properties.

THEOREM 3.11 (one-dimensional (1D) gLF splitting). *If* $\hat{\mathbf{U}} = (\hat{D}, \hat{\boldsymbol{m}}^\top, \hat{E})^\top \in \Omega_\sigma$ *and* $\check{\mathbf{U}} = (\check{D}, \check{\boldsymbol{m}}^\top, \check{E})^\top \in \Omega_\sigma$, *then for any* $\alpha \geq c = 1$ *and any given* $i \in \{1, \ldots, d\}$, *it holds that*

$$\mathbf{G}_{i,\alpha}(\hat{\mathbf{U}}, \check{\mathbf{U}}) := \frac{1}{2}\left(\hat{\mathbf{U}} - \frac{\mathbf{F}_i(\hat{\mathbf{U}})}{\alpha} + \check{\mathbf{U}} + \frac{\mathbf{F}_i(\check{\mathbf{U}})}{\alpha}\right) \in \Omega_\sigma. \tag{3.20}$$

Proof. The first component of $\mathbf{G}_{i,\alpha}$ equals $\frac{1}{2}\big(\hat{D}\big(1-\frac{\hat{v}_i}{\alpha}\big) + \check{D}\big(1+\frac{\check{v}_i}{\alpha}\big)\big) > 0$. With the help of Theorem 3.9, we obtain, for any $\boldsymbol{v}_* \in \mathbb{B}_1(\mathbf{0})$ and any $\rho_* \in \mathbb{R}^+$, that

$$\begin{aligned}
2\varphi_\sigma\big(\mathbf{G}_{i,\alpha}; \boldsymbol{v}_*, \rho_*\big) &= \varphi_\sigma\left(\mathbf{U} - \frac{\mathbf{F}_i(\mathbf{U})}{\alpha}; \boldsymbol{v}_*, \rho_*\right) - \mathrm{e}^\sigma \frac{v_{i,*}\rho_*^\Gamma}{\alpha} + \varphi_\sigma\left(\mathbf{U} + \frac{\mathbf{F}_i(\mathbf{U})}{\alpha}; \boldsymbol{v}_*, \rho_*\right) \\
&\quad + \mathrm{e}^\sigma \frac{v_{i,*}\rho_*^\Gamma}{\alpha} \geq 0,
\end{aligned}$$

[2]Subtracting the right-hand side terms from the left-hand side terms leads to $-(a_2 - b_2 - a_1b_2 + a_2b_1)^2 \leq 0$.

where we have used the linearity of $\varphi_\sigma(\mathbf{U};\boldsymbol{v}_*,\rho_*)$ with respect to $\mathbf{U}$. Then, using Theorem 3.3 concludes that $\mathbf{G}_{i,\alpha}\in\Omega_\sigma^{(2)}=\Omega_\sigma$. ∎

Remark 3.12. Another approach to show Theorem 3.11 is based on the assumption that the exact Riemann solver preserves the invariant domain, which is reasonable but not yet proven for RHD. Our present analysis approach is rigorous, does not rely on any assumption, and would motivate the further study of IRP schemes for some complicated physical systems such as the MHD equations.

Next, we present the multidimensional gLF splitting property on a general polygonal or polyhedron cell. For any vector $\boldsymbol{\xi}=(\xi_1,\dots,\xi_d)^\top\in\mathbb{R}^d$, we define $\boldsymbol{\xi}\cdot\mathbf{F}(\mathbf{U}):=\sum_{k=1}^d\xi_k\mathbf{F}_k(\mathbf{U})$.

THEOREM 3.13. *For $1\le j\le N$, let $s_j>0$ and the unit vector $\boldsymbol{\xi}^{(j)}=(\xi_1^{(j)},\dots,\xi_d^{(j)})^\top$ satisfy*

$$\sum_{j=1}^N s_j\boldsymbol{\xi}^{(j)}=\mathbf{0}. \tag{3.21}$$

Given admissible states $\mathbf{U}^{(ij)}\in\Omega_\sigma$, $1\le i\le Q$, $1\le j\le N$, then for any $\alpha\ge c=1$, it holds that

$$\overline{\mathbf{U}}:=\frac{1}{\sum_{j=1}^N s_j}\sum_{j=1}^N\sum_{i=1}^Q s_j\omega_i\left(\mathbf{U}^{(ij)}-\frac{1}{\alpha}\boldsymbol{\xi}^{(j)}\cdot\mathbf{F}(\mathbf{U}^{(ij)})\right)\in\Omega_\sigma, \tag{3.22}$$

where $\{\omega_i\}_{i=1}^Q$ are all positive with $\sum_{i=1}^Q\omega_i=1$.

Proof. Let $\mathbf{Q}_{\boldsymbol{\xi}}^{(j)}\in\mathbb{R}^{d\times d}$ be a rotational matrix associated with the unit vector $\boldsymbol{\xi}^{(j)}$ and satisfying

$$\mathbf{e}_1^\top\mathbf{Q}_{\boldsymbol{\xi}}^{(j)}=(\boldsymbol{\xi}^{(j)})^\top, \tag{3.23}$$

where $\mathbf{e}_1=(1,\mathbf{0}_{d-1}^\top)^\top$, and $\mathbf{0}_{d-1}$ denotes the zero vector in $\mathbb{R}^{d-1}$. It can be verified that the system (1.1) satisfies the following rotational invariance property:

$$\boldsymbol{\xi}^{(j)}\cdot\mathbf{F}(\mathbf{U}^{(ij)})=\mathbf{Q}_j^{-1}\mathbf{F}_1(\mathbf{Q}_j\mathbf{U}^{(ij)}), \tag{3.24}$$

where $\mathbf{Q}_j:=\mathrm{diag}\{1,\mathbf{Q}_{\boldsymbol{\xi}}^{(j)},1\}$. Notice that the matrix $\mathbf{Q}_{\boldsymbol{\xi}}^{(j)}$ is orthogonal. For any fixed j and any $\boldsymbol{v}_*\in\mathbb{B}_1(\mathbf{0})$, define $\widehat{\boldsymbol{v}}_*:=\mathbf{Q}_{\boldsymbol{\xi}}^{(j)}\boldsymbol{v}_*\in\mathbb{B}_1(\mathbf{0})$. Utilizing (3.23) gives

$$\widehat{v}_{1,*}=\mathbf{e}_1^\top\boldsymbol{v}_*=\mathbf{e}_1^\top\mathbf{Q}_{\boldsymbol{\xi}}^{(j)}\boldsymbol{v}_*=\boldsymbol{\xi}^{(j)}\cdot\boldsymbol{v}_*. \tag{3.25}$$

For $\mathbf{U}^{(ij)}\in\Omega_\sigma$, with the aid of the first equivalent form $\Omega_\sigma^{(1)}$ in (3.2), one can verify that $\widehat{\mathbf{U}}^{(ij)}:=\mathbf{Q}_j\mathbf{U}^{(ij)}\in\Omega_\sigma^{(1)}=\Omega_\sigma$. For any $\boldsymbol{v}_*\in\mathbb{B}_1(\mathbf{0})$ and any $\rho_*>0$, we have

$$\begin{aligned}
&\varphi_\sigma\left(\mathbf{U}^{(ij)}-\alpha^{-1}\boldsymbol{\xi}^{(j)}\cdot\mathbf{F}(\mathbf{U}^{(ij)});\boldsymbol{v}_*,\rho_*\right)-\alpha^{-1}\mathrm{e}^\sigma\left(\boldsymbol{\xi}^{(j)}\cdot\boldsymbol{v}_*\right)\rho_*^\Gamma\\
&=\varphi_\sigma\left(\mathbf{Q}_j^{-1}\widehat{\mathbf{U}}^{(ij)}-\alpha^{-1}\mathbf{Q}_j^{-1}\mathbf{F}_1(\widehat{\mathbf{U}}^{(ij)});(\mathbf{Q}_{\boldsymbol{\xi}}^{(j)})^{-1}\widehat{\boldsymbol{v}}_*,\rho_*\right)-\alpha^{-1}\mathrm{e}^\sigma\widehat{v}_{1,*}\rho_*^\Gamma\\
&=\varphi_\sigma\left(\widehat{\mathbf{U}}^{(ij)}-\alpha^{-1}\mathbf{F}_1(\widehat{\mathbf{U}}^{(ij)});\widehat{\boldsymbol{v}}_*,\rho_*\right)-\alpha^{-1}\mathrm{e}^\sigma\widehat{v}_{1,*}\rho_*^\Gamma\ge 0,
\end{aligned} \tag{3.26}$$

where the first and second steps follow from (3.24)–(3.25) and the orthogonality of $\mathbf{Q}_{\boldsymbol{\xi}}^{(j)}$, respectively, and the inequality follows from Theorem 3.9 for $\widehat{\mathbf{U}}^{(ij)} \in \Omega_\sigma$, $\widehat{\boldsymbol{v}}_* \in \mathbb{B}_1(\mathbf{0})$, $\rho_* \in \mathbb{R}^+$, and $\theta = \alpha^{-1}$. Thus

$$\begin{aligned}\left(\sum_{j=1}^{N} s_j\right)\varphi_\sigma\big(\overline{\mathbf{U}};\boldsymbol{v}_*,\rho_*\big) &= \sum_{j=1}^{N}\sum_{i=1}^{Q} s_j\omega_i\varphi_\sigma\left(\mathbf{U}^{(ij)} - \alpha^{-1}\boldsymbol{\xi}^{(j)}\cdot\mathbf{F}(\mathbf{U}^{(ij)});\boldsymbol{v}_*,\rho_*\right)\\ &\geq \alpha^{-1}\mathrm{e}^{\sigma}\sum_{j=1}^{N}\sum_{i=1}^{Q} s_j\omega_i\left(\boldsymbol{\xi}^{(j)}\cdot\boldsymbol{v}_*\right)\rho_*^{\Gamma}\\ &= \alpha^{-1}\mathrm{e}^{\sigma}\rho_*^{\Gamma}\left(\sum_{j=1}^{N} s_j\boldsymbol{\xi}^{(j)}\right)\cdot\boldsymbol{v}_* = 0,\end{aligned}$$

where we have used the linearity of $\varphi_\sigma(\mathbf{U};\boldsymbol{v}_*,\rho_*)$ with respect to $\mathbf{U}$, the inequality (3.26), and the condition (3.21). Therefore, $\varphi_\sigma(\overline{\mathbf{U}};\boldsymbol{v}_*,\rho_*) \geq 0$ for any $\boldsymbol{v}_* \in \mathbb{B}_1(\mathbf{0})$ and any $\rho_* > 0$. Note that the first component of $\overline{\mathbf{U}}$ equals

$$\begin{aligned}&\frac{1}{\sum_{j=1}^{N} s_j}\sum_{j=1}^{N}\sum_{i=1}^{Q} s_j\omega_i D^{(ij)}\left(1 - \frac{1}{\alpha}\boldsymbol{\xi}^{(j)}\cdot\boldsymbol{v}^{(ij)}\right)\\ \geq\ &\frac{1}{\sum_{j=1}^{N} s_j}\sum_{j=1}^{N}\sum_{i=1}^{Q} s_j\omega_i D^{(ij)}\left(1 - \frac{\|\boldsymbol{v}^{(ij)}\|}{\alpha}\right) > 0.\end{aligned}$$

Hence, $\overline{\mathbf{U}} \in \Omega_\sigma^{(2)}$. Thanks to Theorem 3.3, we have $\overline{\mathbf{U}} \in \Omega_\sigma$, which completes the proof. ∎

As two special cases of Theorem 3.13, the following corollaries show the gLF splitting properties on 2D and three-dimensional (3D) Cartesian mesh cells.

COROLLARY 3.14. *If $\bar{\mathbf{U}}^i$, $\tilde{\mathbf{U}}^i$, $\hat{\mathbf{U}}^i$, $\check{\mathbf{U}}^i \in \Omega_\sigma$ for $i = 1,\ldots,Q$, then for any $\alpha \geq c = 1$, it holds that*

$$\overline{\mathbf{U}} := \frac{1}{2\left(\frac{1}{\Delta x}+\frac{1}{\Delta y}\right)}\sum_{i=1}^{Q}\omega_i\left(\frac{\mathbf{G}_{1,\alpha}(\bar{\mathbf{U}}^i,\tilde{\mathbf{U}}^i)}{\Delta x} + \frac{\mathbf{G}_{2,\alpha}(\hat{\mathbf{U}}^i,\check{\mathbf{U}}^i)}{\Delta y}\right) \in \Omega_\sigma, \tag{3.27}$$

where $\Delta x > 0, \Delta y > 0$, and $\{\omega_i\}_{i=1}^{Q}$ are all positive with $\sum_{i=1}^{Q}\omega_i = 1$.

COROLLARY 3.15. *If $\bar{\mathbf{U}}^i$, $\tilde{\mathbf{U}}^i$, $\hat{\mathbf{U}}^i$, $\check{\mathbf{U}}^i$, $\acute{\mathbf{U}}^i$, $\grave{\mathbf{U}}^i \in \Omega_\sigma$ for $i = 1,\ldots,Q$, then for any $\alpha \geq 1$, it holds that*

$$\begin{aligned}\overline{\mathbf{U}} := &\frac{1}{2\left(\frac{1}{\Delta x}+\frac{1}{\Delta y}+\frac{1}{\Delta z}\right)}\sum_{i=1}^{Q}\omega_i\\ &\cdot\left(\frac{\mathbf{G}_{1,\alpha}(\bar{\mathbf{U}}^i,\tilde{\mathbf{U}}^i)}{\Delta x} + \frac{\mathbf{G}_{2,\alpha}(\hat{\mathbf{U}}^i,\check{\mathbf{U}}^i)}{\Delta y} + \frac{\mathbf{G}_{3,\alpha}(\acute{\mathbf{U}}^i,\grave{\mathbf{U}}^i)}{\Delta z}\right) \in \Omega_\sigma,\end{aligned} \tag{3.28}$$

where $\Delta x > 0, \Delta y > 0, \Delta z > 0$, and $\{\omega_i\}_{i=1}^{Q}$ are all positive with $\sum_{i=1}^{Q}\omega_i = 1$.

4. One-dimensional invariant-region-preserving schemes. In this section, we apply the above theories to explore IRP schemes for the RHD system (1.1) in one spatial dimension. To avoid confusing subscripts, we will use the symbol x to represent the variable x_1 in (1.1). Let $I_j = [x_{j-\frac{1}{2}}, x_{j+\frac{1}{2}}]$, and let $\cup_j I_j$ be a partition of the spatial domain Σ. Denote $\Delta x_j = x_{j+\frac{1}{2}} - x_{j-\frac{1}{2}}$. Assume that the time interval is divided into the mesh $\{t_n\}_{n=0}^{N_t}$ with $t_0 = 0$ and the time step-size Δt determined by the certain CFL condition. We use $\overline{\mathbf{U}}_j^n$ to denote the numerical approximation to the cell average of the exact solution $\mathbf{U}(x,t)$ over I_j at $t = t_n$. Let $\mathbf{U}_0(x) := \mathbf{U}(x,0)$ be an initial solution, and let $S_0 := \min_x S(\mathbf{U}_0(x))$. We are interested in numerical schemes preserving $\overline{\mathbf{U}}_j^n \in \Omega_{S_0}$ for the system. Note that the initial cell average $\overline{\mathbf{U}}_j^0 \in \Omega_{S_0}$ for all j, according to the following lemma (the proof is provided in section SM5 of the supplementary material).

LEMMA 4.1. *Assume that $\mathbf{U}_0(x)$ is an (admissible) initial data of the RHD system (1.1) on the domain Σ, i.e., it satisfies $\mathbf{U}_0(x) \in \mathcal{G}$ for all $x \in \Sigma$. For any $I \subseteq \Sigma$, we have $\overline{\mathbf{U}}_I := \frac{1}{|I|}\int_I \mathbf{U}_0(x)\mathrm{d}x \in \Omega_{S_0}$, where $|I| = \int_I \mathrm{d}x > 0$, and $S_0 = \min_x S(\mathbf{U}_0(x))$.*

4.1. First-order scheme. Consider the first-order LF type scheme

$$\overline{\mathbf{U}}_j^{n+1} = \overline{\mathbf{U}}_j^n - \frac{\Delta t}{\Delta x_j}\Big(\widehat{\mathbf{F}}_1(\overline{\mathbf{U}}_j^n, \overline{\mathbf{U}}_{j+1}^n) - \widehat{\mathbf{F}}_1(\overline{\mathbf{U}}_{j-1}^n, \overline{\mathbf{U}}_j^n)\Big), \tag{4.1}$$

where the numerical flux $\widehat{\mathbf{F}}_1(\cdot,\cdot)$ is defined by

$$\widehat{\mathbf{F}}_1(\mathbf{U}^-, \mathbf{U}^+) = \frac{1}{2}\Big(\mathbf{F}_1(\mathbf{U}^-) + \mathbf{F}_1(\mathbf{U}^+) - \alpha(\mathbf{U}^+ - \mathbf{U}^-)\Big), \tag{4.2}$$

and α denotes the numerical viscosity parameter, which can be taken as $\alpha = c = 1$, a simple upper bound of all wave speeds in the theory of special relativity.

LEMMA 4.2. *If $\overline{\mathbf{U}}_{j-1}^n$, $\overline{\mathbf{U}}_j^n$, and $\overline{\mathbf{U}}_{j+1}^n$ all belong to Ω_σ for certain σ, then the state $\overline{\mathbf{U}}_j^{n+1}$, computed by the scheme (4.1) under the CFL condition*

$$\alpha\Delta t \le \Delta x_j, \tag{4.3}$$

belongs to Ω_σ.

Proof. We rewrite the scheme (4.1) as $\overline{\mathbf{U}}_j^{n+1} = (1-\lambda)\overline{\mathbf{U}}_j^n + \lambda\mathbf{G}_{1,\alpha}(\overline{\mathbf{U}}_{j+1}^n, \overline{\mathbf{U}}_{j-1}^n)$, where $\mathbf{G}_{1,\alpha}$ is defined in (3.20), and $\lambda := \alpha\Delta t/\Delta x_j \in (0,1]$. Thanks to Theorem 3.11, we have $\mathbf{G}_{1,\alpha}(\overline{\mathbf{U}}_{j+1}^n, \overline{\mathbf{U}}_{j-1}^n) \in \Omega_\sigma$, which leads to $\overline{\mathbf{U}}_j^{n+1} \in \Omega_\sigma$ by the convexity of Ω_σ (Lemma 3.7). ∎

Lemma 4.2 implies a discrete (local) minimum entropy principle of the scheme (4.1).

THEOREM 4.3. *If $\overline{\mathbf{U}}_{j-1}^n$, $\overline{\mathbf{U}}_j^n$, and $\overline{\mathbf{U}}_{j+1}^n$ all belong to $\mathcal{G}$, then the state $\overline{\mathbf{U}}_j^{n+1}$, computed by the scheme (4.1) under the CFL condition (4.3), belongs to $\mathcal{G}$ and satisfies $S(\overline{\mathbf{U}}_j^{n+1}) \ge \min\big\{S(\overline{\mathbf{U}}_{j-1}^n), S(\overline{\mathbf{U}}_j^n), S(\overline{\mathbf{U}}_{j+1}^n)\big\}$.*

Proof. By Lemma 4.2 with $\sigma = \min_{j-1\le k\le j+1} S(\overline{\mathbf{U}}_k^n)$, one directly draws the conclusion. ∎

The IRP property of the scheme (4.1) is shown in the following theorem.

THEOREM 4.4. *Under condition (4.3), the scheme (4.1) preserves $\overline{\mathbf{U}}_j^n \in \Omega_{S_0}$ for all j and $n \ge 0$.*

Proof. We prove this by the mathematical induction for the time level number n. By Lemma 4.1, we have $\overline{\mathbf{U}}_j^0 \in \Omega_{S_0}$ for all j, i.e., the conclusion holds for $n = 0$. If we assume that $\overline{\mathbf{U}}_j^n \in \Omega_{S_0}$ for all j, then, by Lemma 4.2 with $\sigma = S_0$, we have $\overline{\mathbf{U}}_j^{n+1} \in \Omega_{S_0}$ for all j. ∎

4.2. High-order schemes. This section studies the high-order IRP methods for 1D RHD equations. We first adopt the forward Euler method for the discretization in time, and will discuss high-order time discretization later. For spatial discretization, we consider the high-order finite volume schemes as well as the scheme satisfied by the cell averages of a standard DG method. The fully discrete schemes can be written into a unified form:

$$\overline{\mathbf{U}}_j^{n+1} = \overline{\mathbf{U}}_j^n - \frac{\Delta t}{\Delta x_j}\Big(\widehat{\mathbf{F}}_1(\mathbf{U}^-_{j+\frac{1}{2}}, \mathbf{U}^+_{j+\frac{1}{2}}) - \widehat{\mathbf{F}}_1(\mathbf{U}^-_{j-\frac{1}{2}}, \mathbf{U}^+_{j-\frac{1}{2}})\Big), \tag{4.4}$$

where $\widehat{\mathbf{F}}_1(\cdot,\cdot)$ is taken as the LF flux in (4.2), and $\mathbf{U}^{\pm}_{j+\frac{1}{2}} = \lim_{\epsilon\to 0^{\pm}} \mathbf{U}_h\big(x_{j+\frac{1}{2}} + \epsilon\big)$. Here $\mathbf{U}_h(x)$ is a piecewise polynomial vector function of degree k, i.e.,

$$\mathbf{U}_h \in \mathbb{V}_h^k := \Big\{\mathbf{u} = (u_1, \ldots, u_{d+2})^\top : \ u_\ell\big|_{I_j} \in \mathbb{P}^k \ \forall \ell, j\Big\},$$

with $\mathbb{P}^k$ denoting the space of polynomials of degree up to k. Specifically, the function $\mathbf{U}_h(x)$ with $\int_{I_j} \mathbf{U}_h \mathrm{d}x = \overline{\mathbf{U}}_j^n$ is an approximation to $\mathbf{U}(x, t_n)$ within I_j. For the finite volume methods, $\mathbf{U}_h(x)$ is reconstructed from $\{\overline{\mathbf{U}}_j^n\}$. For the DG methods, $\mathbf{U}(x, t_n)$ is the piecewise polynomial DG solution, and $\overline{\mathbf{U}}_j^n$ is the first "moment" of $\mathbf{U}(x, t_n)$. Here we omit the DG evolution equations for the high-order "moments" of $\mathbf{U}(x, t_n)$ and the specific reconstruction techniques in the finite volume methods because they are independent of the IRP analyses and limiting techniques presented later.

4.2.1. Theoretical IRP analysis. If the polynomial degree $k = 0$, i.e., $\mathbf{U}_h(x) = \overline{\mathbf{U}}_j^n \ \forall x \in I_j$, then the scheme (4.4) reduces to the first-order scheme (4.1), which is IRP under the CFL condition (4.3). When $k \geq 1$, the solution $\overline{\mathbf{U}}_j^{n+1}$ computed by the high-order accurate scheme (4.4) is not necessarily located in the invariant domain Ω_{S_0} even if $\overline{\mathbf{U}}_j^n \in \Omega_{S_0}$ for all j. In Theorem 4.5, we derive a satisfiable condition which provably ensures the IRP property of the scheme (4.4) with $k \geq 1$.

Let $\{\widehat{x}_j^{(\mu)}, \widehat{\omega}_\mu\}_{\mu=1}^L$ be the L-point Gauss–Lobatto quadrature nodes in I_j and associated weights with $\sum_{\mu=1}^L \widehat{\omega}_\mu = 1$. In addition, we require $2L - 3 \geq k$ and, in particular, take $L = \lceil \frac{k+3}{2} \rceil$.

THEOREM 4.5. *If the piecewise polynomial vector function* $\mathbf{U}_h$ *satisfies*

$$\mathbf{U}_h(\widehat{x}_j^{(\mu)}) \in \Omega_{S_0} \quad \forall \mu \in \{1, 2, \ldots, L\}, \ \forall j, \tag{4.5}$$

then, under the CFL condition

$$\frac{\alpha \Delta t}{\Delta x_j} \leq \widehat{\omega}_1 = \frac{1}{L(L-1)}, \tag{4.6}$$

the solution $\overline{\mathbf{U}}_j^{n+1}$*, computed by the high-order scheme* (4.4)*, belongs to* Ω_{S_0} *for all* j*.*

Proof. The L-point Gauss–Lobatto quadrature rule with $2L - 3 \geq k$ is exact for polynomials of degree k or less. This implies $\overline{\mathbf{U}}_j^n = \frac{1}{\Delta x_j}\int_{I_j} \mathbf{U}_h(x)\mathrm{d}x =$

$\sum_{\mu=1}^{L}\widehat{\omega}_\mu \mathbf{U}_h(\widehat{x}_j^{(\mu)})$. Noting that $\widehat{\omega}_1=\widehat{\omega}_L$ and $\widehat{x}_j^{1,L}=\mathtt{x}_{j\mp\frac{1}{2}}$, we can then reformulate the scheme (4.4) into a form of convex combination:

$$\overline{\mathbf{U}}_j^{n+1}=\sum_{\mu=2}^{L-1}\widehat{\omega}_\mu \mathbf{U}_h(\widehat{\mathtt{x}}_j^{(\mu)})+(\widehat{\omega}_1-\lambda)\left(\mathbf{U}^+_{j-\frac{1}{2}}+\mathbf{U}^-_{j+\frac{1}{2}}\right)+\lambda\Xi_-+\lambda\Xi_+, \tag{4.7}$$

where $\lambda=\alpha\Delta t_n/\Delta x\in(0,\widehat{\omega}_1]$ and

$$\Xi_\pm=\frac{1}{2}\left(\mathbf{U}^\pm_{j+\frac{1}{2}}-\frac{\mathbf{F}_1(\mathbf{U}^\pm_{j+\frac{1}{2}})}{\alpha}+\mathbf{U}^\pm_{j-\frac{1}{2}}+\frac{\mathbf{F}_1(\mathbf{U}^\pm_{j-\frac{1}{2}})}{\alpha}\right).$$

According to the gLF splitting property in Theorem 3.11 and $\mathbf{U}^\pm_{j+\frac{1}{2}}\in\Omega_{S_0}$ by (4.5), we obtain $\Xi_\pm\in\Omega_{S_0}$. Using the convexity of Ω_{S_0} (Lemma 3.7), we conclude that $\overline{\mathbf{U}}_j^{n+1}\in\Omega_{S_0}$ from (4.7). ∎

4.2.2. Invariant-region-preserving limiter. In general, the high-order scheme (4.4) does not meet the condition (4.5) automatically. Now, we design a simple limiter to effectively enforce the condition (4.5) without losing high-order accuracy and conservation. Our limiter is motivated by the existing bound-preserving and physical-constraint-preserving limiters (cf. [41, 42, 34, 24, 37, 28]).

Before presenting the limiter, we define $q(\mathbf{U}):=E-\sqrt{D^2+\|\boldsymbol{m}\|^2}$; then the second constraint in (3.2) becomes $q(\mathbf{U})>0$. As observed in [34], the function $q(\mathbf{U})$ is strictly concave. This function will play an important role in our limiter.

Denote $\mathbb{X}_j:=\{\widehat{x}_j^{(\mu)}\}_{\mu=1}^L$ and

$$\overline{\mathbb{V}}_h^k:=\left\{\mathbf{u}\in\mathbb{V}_h^k:\ \ \frac{1}{\Delta x_j}\int_{I_j}\mathbf{u}(x)\mathrm{d}x\in\Omega_{S_0}\ \forall j\right\},$$
$$\widetilde{\mathbb{V}}_h^k:=\left\{\mathbf{u}\in\mathbb{V}_h^k:\ \ \mathbf{u}\big|_{I_j}(x)\in\Omega_{S_0}\ \forall x\in\mathbb{X}_j,\ \forall j\right\}.$$

For any $\mathbf{U}_h\in\overline{\mathbb{V}}_h^k$ with $\mathbf{U}_h\big|_{I_j}=:\mathbf{U}_j(x)=\big(D_j(x),m_j(x),E_j(x)\big)^\top$, we define the IRP limiting operator $\Pi_h:\overline{\mathbb{V}}_h^k\to\widetilde{\mathbb{V}}_h^k$ by

$$\Pi_h\mathbf{U}_h\big|_{I_j}=\widetilde{\mathbf{U}}_j(x)\quad\forall j, \tag{4.8}$$

with the limited polynomial vector function $\widetilde{\mathbf{U}}_j(x)$ constructed via the following three steps.

Step (i). First, modify the density to enforce its positivity via

$$\widehat{D}_j(x)=\theta_1\left(D_j(x)-\overline{D}_j^n\right)+\overline{D}_j^n,\qquad \theta_1:=\min\left\{1,\left|\frac{\overline{D}_j^n-\varepsilon_1}{\overline{D}_j^n-\min_{x\in\mathbb{X}_j}D_j(x)}\right|\right\}, \tag{4.9}$$

where ε_1 is a small positive number as the desired lower bound for density, is introduced to avoid the effect of the round-off error, and can be taken as $\varepsilon_1=\min\{10^{-13},\overline{D}_j^n\}$.

Step (ii). Then, modify $\widehat{\mathbf{U}}_j(x)=\big(\widehat{D}_j(x),m_j(x),E_j(x)\big)^\top$ to enforce the positivity of $q(\mathbf{U})$ via

$$\breve{\mathbf{U}}_j(x)=\theta_2\left(\widehat{\mathbf{U}}_j(x)-\overline{\mathbf{U}}_j^n\right)+\overline{\mathbf{U}}_j^n, \tag{4.10}$$

$$\theta_2 := \min\left\{1, \left|\frac{q(\overline{\mathbf{U}}_j) - \varepsilon_2}{q(\overline{\mathbf{U}}_j^n) - \min_{x\in\mathbb{X}_j} q(\widehat{\mathbf{U}}_j(x))}\right|\right\},$$

where ε_2 is a small positive number as the desired lower bound for $q(\mathbf{U})$, is introduced to avoid the effect of the round-off error, and can be taken as $\varepsilon_2 = \min\{10^{-13}, q(\overline{\mathbf{U}}_j^n)\}$.

Step (iii). Finally, modify $\breve{\mathbf{U}}_j(x)$ to enforce the entropy principle $S(\mathbf{U}) \geq S_0$ via

$$\widetilde{\mathbf{U}}_j(x) = \theta_3\left(\breve{\mathbf{U}}_j(x) - \overline{\mathbf{U}}_j^n\right) + \overline{\mathbf{U}}_j^n, \qquad \theta_3 := \min_{x\in\mathbb{X}_j} \tilde{\theta}(x), \tag{4.11}$$

where, for $x \in \{x \in \mathbb{X}_j : S(\breve{\mathbf{U}}_j(x)) \geq S_0\}$, $\tilde{\theta}(x) = 1$, and, for $x \in \{x \in \mathbb{X}_j : S(\breve{\mathbf{U}}_j(x)) < S_0\}$, $\tilde{\theta}(x)$ is the (unique) solution to the nonlinear equation

$$S\Big((1-\tilde{\theta})\overline{\mathbf{U}}_j^n + \tilde{\theta}\,\breve{\mathbf{U}}_j(x)\Big) = S_0, \qquad \tilde{\theta} \in [0,1).$$

The limiter Π_h is a combination of the bound-preserving limiter (4.9)–(4.10) (cf. [24]) and the *entropy limiter* (4.11). According to the above definition of the limiter Π_h and the Jensen's inequality for the concave function $q(\mathbf{U})$, we immediately obtain the following proposition.

PROPOSITION 4.6. *For any* $\mathbf{U}_h \in \overline{\mathbb{V}}_h^k$, *one has* $\Pi_h\mathbf{U}_h \in \widetilde{\mathbb{V}}_h^k$.

Proposition 4.6 indicates that the limited solution (4.8) satisfies the condition (4.5). Note that this type of local scaling limiters keep the conservation $\int_{I_j} \Pi_h(\mathbf{u})\mathrm{d}x = \int_{I_j} \mathbf{u}\mathrm{d}x\ \forall \mathbf{u} \in \overline{\mathbb{V}}_h^k$ and do not destroy the high-order accuracy; see [40, 41, 39] for details.

Remark 4.7. The invariant region Ω_{S_0} can also be reformulated as

$$\Omega_{S_0}^{(1)} = \left\{\mathbf{U} = (D, \boldsymbol{m}^\top, E)^\top \in \mathbb{R}^{d+2} :\ D > 0,\ q(\mathbf{U}) > 0,\ \widetilde{q}(\mathbf{U}) \geq 0\right\},$$

where $\widetilde{q}(\mathbf{U}) := D(S(\mathbf{U}) - S_0)$, and we have used $D > 0$ to reformulate the third constraint $S(\mathbf{U}) \geq S_0$ in (3.2). Thanks to Proposition 2.1, the function $\widetilde{q}(\mathbf{U})$ is strictly concave for $\mathbf{U} \in \mathcal{G}$. Motivated by this property and [16], we can also construct another (simpler but possibly more restrictive) approach to enforce the entropy principle $S(\mathbf{U}) \geq S_0$ by modifying $\breve{\mathbf{U}}_j(x)$ to

$$\widetilde{\mathbf{U}}_j(x) = \tilde{\theta}_3\left(\breve{\mathbf{U}}_j(x) - \overline{\mathbf{U}}_j^n\right) + \overline{\mathbf{U}}_j^n, \qquad \tilde{\theta}_3 := \min\left\{1, \left|\frac{\widetilde{q}(\overline{\mathbf{U}}_j^n)}{\widetilde{q}(\overline{\mathbf{U}}_j^n) - \min_{x\in\mathbb{X}_j} \widetilde{q}(\breve{\mathbf{U}}_j(x))}\right|\right\}.$$

With the aid of the IRP limiter Π_h defined in (4.8), we modify the high-order scheme (4.4) into

$$\overline{\mathbf{U}}_j^{n+1} = \overline{\mathbf{U}}_j^n - \frac{\Delta t}{\Delta x_j}\Big(\widehat{\mathbf{F}}_1(\widetilde{\mathbf{U}}_{j+\frac{1}{2}}^-, \widetilde{\mathbf{U}}_{j+\frac{1}{2}}^+) - \widehat{\mathbf{F}}_1(\widetilde{\mathbf{U}}_{j-\frac{1}{2}}^-, \widetilde{\mathbf{U}}_{j-\frac{1}{2}}^+)\Big) =: \overline{\mathbf{U}}_j^n + \Delta t\mathbf{L}_j(\Pi_h\mathbf{U}_h), \tag{4.12}$$

where $\widetilde{\mathbf{U}}_{j+\frac{1}{2}}^{\pm} = \lim_{\epsilon\to 0^\pm} \Pi_h\mathbf{U}_h\big(x_{j+\frac{1}{2}} + \epsilon\big)$. Based on Theorem 4.5 and Proposition 4.6, we know that the scheme (4.12) is IRP under the CFL condition (4.6).

The scheme (4.12) is only of first-order accuracy in time. To achieve IRP schemes of high-order accuracy in both time and space, we can use any high-order accurate

strong-stability-preserving (SSP) methods [4] to replace the forward Euler time discretization in (4.12). For instance, the widely used third-order SSP Runge–Kutta (SSP-RK) method can be used

$$\begin{cases} \overline{\mathbf{U}}_j^* = \overline{\mathbf{U}}_j^n + \Delta t \mathbf{L}_j(\Pi_h \mathbf{U}_h), \\ \overline{\mathbf{U}}_j^{**} = \frac{3}{4}\overline{\mathbf{U}}_j^n + \frac{1}{4}\Big(\overline{\mathbf{U}}_j^* + \Delta t \mathbf{L}_j(\Pi_h \mathbf{U}_h^*)\Big), \\ \overline{\mathbf{U}}_j^{n+1} = \frac{1}{3}\overline{\mathbf{U}}_j^n + \frac{2}{3}\Big(\overline{\mathbf{U}}_j^{**} + \Delta t \mathbf{L}_j(\Pi_h \mathbf{U}_h^{**})\Big), \end{cases} \tag{4.13}$$

as well as the third-order accurate SSP multistep (SSP-MS) method,

$$\overline{\mathbf{U}}_j^{n+1} = \frac{16}{27}(\overline{\mathbf{U}}_j^n + 3\Delta t \mathbf{L}_j(\Pi_h \mathbf{U}_h^n)) + \frac{11}{27}\left(\overline{\mathbf{U}}_j^{n-3} + \frac{12}{11}\Delta t \mathbf{L}_j(\Pi_h \mathbf{U}_h^{n-3})\right). \tag{4.14}$$

Since SSP methods are formally convex combinations of the forward Euler method, the resulting high-order schemes (4.13) and (4.14) are still IRP, according to the convexity of Ω_{S_0} (Lemma 3.7).

5. Multidimensional invariant-region-preserving schemes. In this section, we study IRP schemes for the 2D RHD equations, while keeping in mind that our IRP analyses and proposed IRP schemes are extensible to the 3D case. Assume that the physical domain Σ in the 2D space is discretized by a mesh $\mathcal{T}_h$. In general, the mesh may be unstructured and consists of polygonal cells. We also partition the time interval into a mesh $\{t_n\}_{n=0}^{N_t}$ with $t_0 = 0$ and the time step-size Δt determined by the certain CFL condition. We will use the capital letter K to denote an arbitrary cell in $\mathcal{T}_h$. Let $\mathscr{E}_K^j$, $j = 1, \ldots, N_K$, denote the edges of K, and let K_j be the adjacent cell sharing the edge $\mathscr{E}_K^j$ with K. We use $\boldsymbol{\xi}_K^{(j)} = \big(\xi_{1,K}^{(j)}, \xi_{2,K}^{(j)}\big)$ to denote the unit normal vector of $\mathscr{E}_K^j$, whose direction points from K to K_j. We use $|\mathscr{E}_K^j|$ and $|K|$ to represent the length of $\mathscr{E}_K^j$ and the area of K, respectively. Let $\overline{\mathbf{U}}_K^n$ denote the numerical approximation to the cell average of the exact solution $\mathbf{U}(\boldsymbol{x}, t)$ over K at $t = t_n$. Define $\mathbf{U}_0(\boldsymbol{x}) := \mathbf{U}(\boldsymbol{x}, 0)$ as the initial data and $S_0 := \min_{\boldsymbol{x}} S(\mathbf{U}_0(\boldsymbol{x}))$. According to Lemma 4.1, the initial cell average $\overline{\mathbf{U}}_K^0$ always belongs to Ω_{S_0} for all $K \in \mathcal{T}_h$. We would like to seek numerical schemes preserving $\overline{\mathbf{U}}_K^n \in \Omega_{S_0}$ for all $K \in \mathcal{T}_h$ and $n \geq 1$.

5.1. First-order scheme. Consider the following first-order scheme on the mesh $\mathcal{T}_h$ for the RHD equations (1.1):

$$\overline{\mathbf{U}}_K^{n+1} = \overline{\mathbf{U}}_K^n - \frac{\Delta t}{|K|}\sum_{j=1}^{N_K} \left|\mathscr{E}_K^j\right| \widehat{\mathbf{F}}\big(\overline{\mathbf{U}}_K^n, \overline{\mathbf{U}}_{K_j}^n; \boldsymbol{\xi}_K^{(j)}\big), \tag{5.1}$$

with the numerical flux $\widehat{\mathbf{F}}$ taken as the LF flux

$$\widehat{\mathbf{F}}\left(\mathbf{U}^-, \mathbf{U}^+; \boldsymbol{\xi}\right) = \frac{1}{2}\Big(\boldsymbol{\xi} \cdot \mathbf{F}(\mathbf{U}^-) + \boldsymbol{\xi} \cdot \mathbf{F}(\mathbf{U}^+) - \alpha(\mathbf{U}^+ - \mathbf{U}^-)\Big), \tag{5.2}$$

where the numerical viscosity parameter α is chosen as the speed of light in vacuum $c = 1$, which is a simple upper bound of all wave speeds in the theory of special relativity.

LEMMA 5.1. *If $\overline{\mathbf{U}}_K^n \in \Omega_\sigma$, $\overline{\mathbf{U}}_{K_j}^n \in \Omega_\sigma$, $1 \leq j \leq N_K$, for certain σ, then the state $\overline{\mathbf{U}}_K^{n+1}$, computed by the scheme* (5.1) *under the CFL condition*

$$\frac{\alpha \Delta t}{2|K|}\sum_{j=1}^{N_K} \left|\mathscr{E}_K^j\right| \leq 1, \tag{5.3}$$

belongs to Ω_σ.

Proof. Substituting the numerical flux (5.2) into the scheme (5.1) and then using the identity $\sum_{j=1}^{N_K} \left|\mathscr{E}_K^j\right| \boldsymbol{\xi}_K^{(j)} = \mathbf{0}$, we rewrite the scheme (5.1) as $\overline{\mathbf{U}}_K^{n+1} = (1-\lambda)\overline{\mathbf{U}}_K^n + \lambda\Xi$, where $\lambda := \frac{\alpha\Delta t}{2|K|}\sum_{j=1}^{N_K}\left|\mathscr{E}_K^j\right| \in (0,1]$ under the condition (5.3), and

$$\Xi := \frac{1}{\sum_{j=1}^{N_K}\left|\mathscr{E}_K^j\right|}\sum_{j=1}^{N_K}\left|\mathscr{E}_K^j\right|\left(\overline{\mathbf{U}}_{K_j}^n - \frac{1}{\alpha}\boldsymbol{\xi}_K^{(j)}\cdot\mathbf{F}\big(\overline{\mathbf{U}}_{K_j}^n\big)\right).$$

Thanks to the gLF splitting property in Theorem 3.13, we have $\Xi \in \Omega_\sigma$, which leads to $\overline{\mathbf{U}}_K^{n+1} \in \Omega_\sigma$ by the convexity of Ω_σ (Lemma 3.7). ∎

Lemma 5.1 implies a discrete (local) minimum entropy principle of the scheme (5.1).

THEOREM 5.2. *If* $\overline{\mathbf{U}}_K^n \in \mathcal{G}$, $\overline{\mathbf{U}}_{K_j}^n \in \mathcal{G}$, $1 \le j \le N_K$, *then the state* $\overline{\mathbf{U}}_K^{n+1}$, *computed by the scheme* (5.1) *under the CFL condition* (5.3), *belongs to* $\mathcal{G}$ *and satisfies*

$$S(\overline{\mathbf{U}}_K^{n+1}) \ge \min\left\{S(\overline{\mathbf{U}}_K^n), \min_{1\le j\le N_K} S(\overline{\mathbf{U}}_{K_j}^n)\right\}.$$

Proof. By Lemma 5.1 with $\sigma = \min\big\{S(\overline{\mathbf{U}}_K^n), \min_{1\le j\le N_K} S(\overline{\mathbf{U}}_{K_j}^n)\big\}$ we directly draw the conclusion. ∎

The IRP property of the scheme (5.1) is shown in the following theorem.

THEOREM 5.3. *Under condition* (5.3), *the scheme* (5.1) *preserves* $\overline{\mathbf{U}}_K^n \in \Omega_{S_0}$ *for all* $K \in \mathcal{T}_h$ *and* $n \ge 0$.

Proof. The conclusion follows from Lemma 5.1 with $\sigma = S_0$ and the principle of mathematical induction for the time level number n. ∎

5.2. High-order schemes. Next, we discuss the IRP high-order schemes for the 2D RHD equations. As in the 1D case, we focus on the time discretization with the forward Euler method, while our IRP techniques and analyses also work for high-order time discretization using the explicit SSP methods, which are formed by convex combinations of the forward Euler method [4].

To achieve $(k+1)$th-order accuracy in space, a piecewise polynomial vector function $\mathbf{U}_h(\boldsymbol{x})$ (i.e., $\mathbf{U}_h|_K$ is a polynomial vector of degree k for all $K \in \mathcal{T}_h$) is also constructed, as an approximation to the exact solution $\mathbf{U}(\boldsymbol{x}, t_n)$. It is either evolved in the DG methods or reconstructed in the finite volume methods from the cell averages $\{\overline{\mathbf{U}}_K^n : K \in \mathcal{T}_h\}$. Moreover, the cell average of $\mathbf{U}_h(\boldsymbol{x})$ over K is equal to $\overline{\mathbf{U}}_K^n$. A high-order finite volume scheme as well as the scheme satisfied by the cell averages of a standard DG method can then be written as

$$\overline{\mathbf{U}}_K^{n+1} = \bar{\mathbf{U}}_K^n - \frac{\Delta t}{|K|}\sum_{j=1}^{N_K}|\mathscr{E}_K^j|\widehat{\mathbf{F}}_{\mathscr{E}_K^j}, \tag{5.4}$$

where $\widehat{\mathbf{F}}_{\mathscr{E}_K^j} = \sum_{\nu=1}^{Q}\omega_\nu\widehat{\mathbf{F}}\big(\mathbf{U}_h^{\mathrm{int}(K)}(\boldsymbol{x}_K^{(j\nu)}), \mathbf{U}_h^{\mathrm{ext}(K)}(\boldsymbol{x}_K^{(j\nu)}); \boldsymbol{\xi}_K^{(j)}\big)$. Here the superscripts "ext(K)" and "int(K)" indicate that the corresponding limits of $\mathbf{U}_h(\boldsymbol{x})$ at the cell edges are taken from the exterior and interior of K, respectively. The numerical flux $\widehat{\mathbf{F}}$ is taken as the LF flux defined in (5.2), and $\{\boldsymbol{x}_K^{(j\nu)}, \omega_\nu\}_{1\le\nu\le Q}$ denotes the Q-point Gauss quadrature nodes and weights on $\mathscr{E}_K^j$. In the following, we derive a satisfiable

condition which provably ensures the IRP property of the high-order accurate scheme (5.4) when the polynomial degree $k \geq 1$. Assume that one can *exactly* decompose the cell average by certain 2D quadrature:

$$\overline{\mathbf{U}}_K^n = \frac{1}{|K|}\int_K \mathbf{U}_h(\boldsymbol{x})\mathrm{d}\boldsymbol{x} = \sum_{j=1}^{N_K}\sum_{\nu=1}^{Q}\varpi_{j\nu}\mathbf{U}_h^{\mathrm{int}(K)}(\boldsymbol{x}_K^{(j\nu)}) + \sum_{\beta=1}^{\widetilde{Q}}\widetilde{\varpi}_\beta\mathbf{U}_h^{\mathrm{int}(K)}(\widetilde{\boldsymbol{x}}_K^{(\beta)}), \tag{5.5}$$

where $\{\widetilde{\boldsymbol{x}}_K^{(\beta)}\}$ are the (possible) involved quadrature points excluding $\{\boldsymbol{x}_K^{(j\nu)}\}$ in the cell K; $\{\varpi_{j\nu}\}$, and $\{\widetilde{\varpi}_\beta\}$ are positive weights satisfying $\sum_{j=1}^{N_K}\sum_{\nu=1}^{Q}\varpi_{j\nu} + \sum_{\beta=1}^{\widetilde{Q}}\widetilde{\varpi}_\beta = 1$. Such a quadrature-based decomposition was first proposed by Zhang and Shu in [40, 41] on rectangular cells by tensor products of Gauss and Gauss–Lobatto quadratures. It can also be designed on triangular cells and more general polygons, as demonstrated in, e.g., [43, 20]. Define

$$\mathbb{X}_K := \left\{\boldsymbol{x}_K^{(j\nu)}\right\}_{1\leq j\leq N_K, 1\leq\nu\leq Q}\bigcup\left\{\widetilde{\boldsymbol{x}}_K^{(\beta)}\right\}_{1\leq\beta\leq\widetilde{Q}}. \tag{5.6}$$

THEOREM 5.4. *If the piecewise polynomial vector function* $\mathbf{U}_h$ *satisfies*

$$\mathbf{U}_h(\boldsymbol{x}) \in \Omega_{S_0} \qquad \forall \boldsymbol{x} \in \mathbb{X}_K, \quad \forall K \in \mathcal{T}_h, \tag{5.7}$$

then, under the CFL condition

$$\alpha\Delta t\frac{|\mathscr{E}_K^j|}{|K|} \leq \min_{1\leq\nu\leq Q}\frac{\varpi_{j\nu}}{\omega_\nu}, \qquad 1 \leq j \leq N_K \quad \forall K \in \mathcal{T}_h, \tag{5.8}$$

the solution $\overline{\mathbf{U}}_K^{n+1}$*, computed by the high-order scheme* (5.4)*, belongs to* Ω_{S_0} *for all* $K \in \mathcal{T}_h$*.*

Proof. Substituting the decomposition (5.5) into (5.4), we can reformulate the scheme (5.4) into a form of convex combination:

$$\begin{aligned}\overline{\mathbf{U}}_K^{n+1} = &\sum_{j=1}^{N_K}\sum_{\nu=1}^{Q}\left(\varpi_{j\nu} - \alpha\Delta t\omega_\nu\frac{|\mathscr{E}_K^j|}{|K|}\right)\mathbf{U}_h^{\mathrm{int}(K)}(\boldsymbol{x}_K^{(j\nu)}) \\ &+ \sum_{\beta=1}^{\widetilde{Q}}\widetilde{\varpi}_\beta\mathbf{U}_h^{\mathrm{int}(K)}(\widetilde{\boldsymbol{x}}_K^{(\beta)}) + \frac{\alpha\Delta t}{2|K|}\left(\sum_{j=1}^{N}|\mathscr{E}_K^j|\right)\left(\Xi^{\mathrm{int}(K)} + \Xi^{\mathrm{ext}(K)}\right),\end{aligned} \tag{5.9}$$

with

$$\Xi^{\mathrm{int}(K)} := \frac{1}{\sum_{j=1}^{N_K}|\mathscr{E}_K^j|}\sum_{j=1}^{N_K}\sum_{\nu=1}^{Q}|\mathscr{E}_K^j|\omega_\nu\left(\mathbf{U}_h^{\mathrm{int}(K)}(\boldsymbol{x}_K^{(j\nu)}) - \frac{1}{\alpha}\boldsymbol{\xi}_K^{(j)}\cdot\mathbf{F}\left(\mathbf{U}_h^{\mathrm{int}(K)}(\boldsymbol{x}_K^{(j\nu)})\right)\right),$$

$$\Xi^{\mathrm{ext}(K)} := \frac{1}{\sum_{j=1}^{N_K}|\mathscr{E}_K^j|}\sum_{j=1}^{N_K}\sum_{\nu=1}^{Q}|\mathscr{E}_K^j|\omega_\nu\left(\mathbf{U}_h^{\mathrm{ext}(K)}(\boldsymbol{x}_K^{(j\nu)}) - \frac{1}{\alpha}\boldsymbol{\xi}_K^{(j)}\cdot\mathbf{F}\left(\mathbf{U}_h^{\mathrm{ext}(K)}(\boldsymbol{x}_K^{(j\nu)})\right)\right).$$

Thanks to the gLF splitting property in Theorem 3.13, under assumption (5.7) we obtain $\Xi^{\mathrm{int}(K)} \in \Omega_{S_0}$ and $\Xi^{\mathrm{ext}(K)} \in \Omega_{S_0}$. Using the convexity of Ω_{S_0} (Lemma 3.7), we conclude $\overline{\mathbf{U}}_K^{n+1} \in \Omega_{S_0}$ from the convex combination form (5.9) under condition (5.8). ∎

Theorem 5.4 provides a sufficient condition (5.7) for the high-order scheme (5.4) to be IRP. The condition (5.7), which is not satisfied automatically in general, can again be enforced by a simple IRP limiting operator Π_h similar to the 1D case; see section 4.2.2, with the 1D point set $\mathbb{X}_j$ replaced by the 2D point set $\mathbb{X}_K$ (5.6) accordingly. With the IRP limiter applied to the approximate solution $\widetilde{\mathbf{U}}_h = \Pi_h \mathbf{U}_h$, the resulting scheme

$$\overline{\mathbf{U}}_K^{n+1} = \bar{\mathbf{U}}_K^n - \frac{\Delta t}{|K|} \sum_{j=1}^{N_K} \sum_{\nu=1}^{Q} |\mathscr{E}_K^j| \omega_\nu \widehat{\mathbf{F}} \left(\widetilde{\mathbf{U}}_h^{\mathrm{int}(K)}(\boldsymbol{x}_K^{(j\nu)}), \widetilde{\mathbf{U}}_h^{\mathrm{ext}(K)}(\boldsymbol{x}_K^{(j\nu)}); \boldsymbol{\xi}_K^{(j)} \right)$$

is IRP and also high-order accurate in space. As in the 1D case, Theorem 5.4 also remains valid if a high-order SSP time discretization [4] is used. Illustration and some details of the 2D IRP schemes on Cartesian meshes can be found in section SM6 of the supplementary material.

6. Numerical tests. In this section, we present numerical tests on several benchmark RHD problems to validate the accuracy and effectiveness of our IRP DG methods on 1D and 2D uniform Cartesian meshes. The third-order SSP-RK method (4.13) or SSP-MS method (4.14) will be employed for time discretization. Unless otherwise stated, we take the adiabatic index as $\Gamma = 5/3$, and set the CFL numbers as 0.3, 0.15, 0.1, respectively, for the second-order (P^1-based), third-order (P^2-based), and fourth-order (P^3-based) DG methods with the SSP-RK time discretization; the CFL numbers for the SSP-MS-DG methods are one-third of those for the SSP-RK-DG methods.

For convenience, we refer to the 1D bound-preserving limiter (4.9)–(4.10) (cf. [24]) as the *BP limiter*. Our IRP limiter (4.9)–(4.11) corresponds to a combination of the BP limiter and the *entropy limiter* (4.11). The same names/abbreviations will also be used for those corresponding limiters in the 2D case. We will compare the numerical results with our IRP limiter and those with only the BP limiter. For testing purposes as in [24, 16], in the simulations we do *not* use any other nonoscillatory limiters (e.g., the TVB or WENO limiters) unless otherwise stated.

6.1. Example 1: 1D smooth problem. To examine the accuracy of our 1D DG methods we first test a smooth problem similar to [24, 37, 41, 42]. The initial conditions are $\rho(x,0) = 1 + 0.99999 \sin\big(2\pi x\big)$, $v(x,0) = 0.9$, $p(x,0) = 1$. The computational domain is taken as $[0,1]$ with periodic boundary conditions, so that the exact solution is $\rho(x,t) = 1 + 0.99999 \sin\big(2\pi(x - 0.9t)\big)$, $v(x,t) = 0.9$, $p(x,t) = 1$. In the computations, the domain is partitioned into N uniform cells with $N \in \{10, 20, 40, 80, 160, 320\}$. For the P^3-based DG method, we take (only in this accuracy test) the time step-sizes as $\Delta t = 0.1 \Delta x^{\frac{4}{3}}$ and $\Delta t = \frac{0.1}{3} \Delta x^{\frac{4}{3}}$ for the third-order SSP-RK and SSP-MS time discretizations, respectively, so as to match the fourth-order accuracy of spatial discretization.

Table 6.1 lists the numerical errors at $t = 0.2$ in the rest-mass density and the corresponding convergence rates for the P^k-based IRP DG methods ($k = 1, 2, 3$) at different grid resolutions. As observed in [42, 24], the accuracy degenerates for SSP-RK and $k \geq 2$, which is due to the lower-order accuracy in the RK intermediate stages as explained in [42]. The desired full order of accuracy is observed for the SSP-MS time discretization, indicating that the IRP limiter itself does not lose the accuracy for smooth solutions as expected from the analyses in [40, 39, 16].

TABLE 6.1

Example 1: Errors at $t = 0.2$ in the rest-mass density for the proposed P^k-based DG methods ($k = 1, 2, 3$), with the SSP-RK or SSP-MS time discretization, at different spatial grid resolutions.

		SSP-RK				SSP-MS			
k	N	l^1 error	Order	l^2 error	Order	l^1 error	Order	l^2 error	Order
1	10	1.75e-2	–	1.98e-2	–	1.72e-2	–	1.96e-2	–
	20	3.16e-3	2.47	4.47e-3	2.14	3.13e-3	2.46	4.41e-3	2.15
	40	8.19e-4	1.95	1.08e-3	2.05	8.19e-4	1.94	1.07e-3	2.05
	80	1.93e-4	2.08	2.49e-4	2.11	1.92e-4	2.09	2.46e-4	2.12
	160	4.63e-5	2.06	5.87e-5	2.08	4.61e-5	2.06	5.84e-5	2.08
	320	1.13e-5	2.04	1.38e-5	2.09	1.12e-5	2.04	1.37e-5	2.09
2	10	1.24e-3	–	1.47e-3	–	7.76e-4	3.21	9.15e-4	3.31
	20	1.83e-4	2.76	2.37e-4	2.63	8.40e-5	3.04	9.24e-5	3.02
	40	2.75e-5	2.74	4.98e-5	2.25	1.02e-5	3.00	1.14e-5	3.00
	80	4.06e-6	2.76	1.03e-5	2.28	1.27e-6	3.00	1.42e-6	3.00
	160	5.90e-7	2.78	2.12e-6	2.28	1.59e-7	3.00	1.77e-7	3.00
	320	9.16e-8	2.69	4.51e-7	2.23	1.99e-8	3.00	2.22e-8	3.00
3	10	6.12e-5	–	8.32e-5	–	1.92e-5	–	2.24e-5	–
	20	4.84e-6	3.66	9.94e-6	3.07	1.29e-6	3.90	1.50e-6	3.90
	40	3.00e-7	4.01	9.89e-7	3.33	7.86e-8	4.04	8.89e-8	4.07
	80	2.71e-8	3.47	1.26e-7	2.97	4.85e-9	4.02	5.48e-9	4.02
	160	2.30e-9	3.55	1.52e-8	3.05	3.04e-10	4.00	3.42e-10	4.00
	320	2.08e-10	3.47	1.84e-9	3.04	1.90e-11	4.00	2.13e-11	4.01

6.2. Example 2: 1D Riemann problem. This example investigates the capability of our methods in resolving discontinuous solutions by testing a 1D Riemann problem in the domain $[0, 1]$ with the following initial conditions:

$$(\rho, v, p)(x, 0) = \begin{cases} (0.8, 0.5, 8), & x < 0.5, \\ (1, 0, 1), & x > 0.5. \end{cases}$$

The solution consists of a left-moving rarefaction wave, a constant discontinuity, and a right-moving shock wave. Figure 6.1 displays the numerical solutions computed by the fourth-order DG methods with the BP or IRP limiter, respectively, on a mesh of 320 uniform cells, against the exact solution. In this simulation, we do *not* use any other nonoscillatory limiters such as the TVB or WENO limiters. We can observe that the numerical results with only the BP limiter exhibit overshoot in the rest-mass density near the contact discontinuity and some small oscillations. When the IRP limiter is applied (i.e., the entropy limiter (4.11) is added), the overshoot and oscillations in the DG solution are damped. This is consistent with the observation in [18, 42, 16] that enforcing the discrete minimum entropy principle could help to suppress numerical oscillations. Figure 6.2 shows the time evolution of the minimum specific entropy values of the DG solutions. It is seen that the minimum remains the same for the DG scheme with the IRP limiter, which indicates that the minimum entropy principle is preserved, while the DG scheme with only the BP limiter fails to keep the principle.

6.3. Example 3: 2D smooth problem. To check the accuracy of our 2D IRP DG methods we simulate a smooth problem from [37], with the initial data $\rho(x, y, 0) = 1 + 0.99999 \sin(2\pi(x + y))$, $\boldsymbol{v}(x, y, 0) = (0.99/\sqrt{2}, 0.99/\sqrt{2})^\top$, $p(x, y, 0) = 10^{-2}$, in the domain $[0, 1]^2$ with periodic boundary conditions. The exact solution is $\rho(x, y, 0) = 1 + 0.99999 \sin(2\pi(x + y - 0.99\sqrt{2}t))$, $\boldsymbol{v}(x, y, t) = (0.99/\sqrt{2}, 0.99/\sqrt{2})^\top$, $p(x, y, t) = 10^{-2}$, which describes the propagation of an RHD sine wave with low

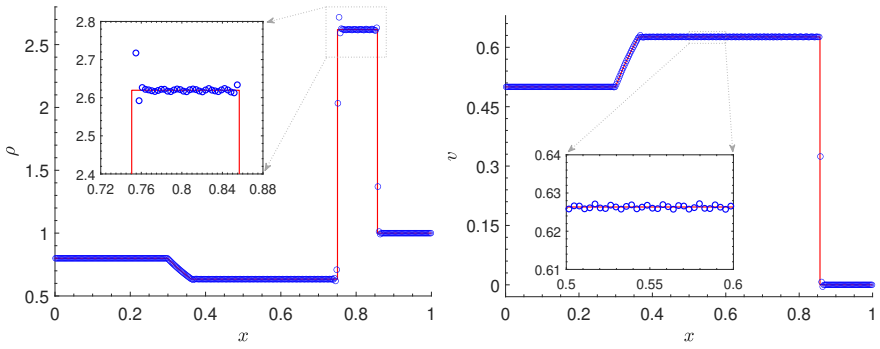

(a) ρ: With the BP limiter (b) v: With the BP limiter

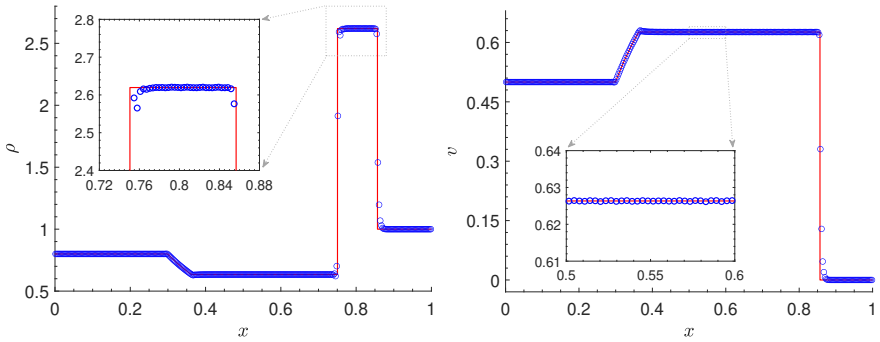

(c) ρ: With the IRP limiter (d) v: With the IRP limiter

FIG. 6.1. *Example* 2*: The computed rest-mass density and velocity (and their close-up) at* $t = 0.4$*. The symbols "∘" denote the numerical solutions obtained by the fourth-order DG methods with the BP limiter or with the IRP limiter on the mesh of* 320 *uniform cells, while the solid lines denote the exact solution. (Here we do not use any other nonoscillatory limiters, e.g., the TVB or WENO limiters.)*

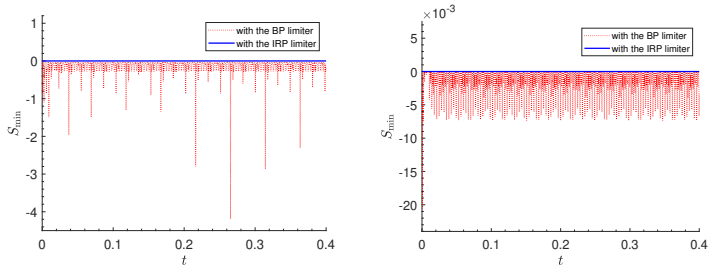

FIG. 6.2. *Example* 2*: Time evolution of* $S_{\min}(t)$ *for the DG solutions with the IRP limiter* (4.9)–(4.11) *or with the BP limiter* (4.9)–(4.10)*. Left:* $S_{\min}(t) = \min_{j,\mu} S(\mathbf{U}_h(\widehat{x}_j^{(\mu)}, t))$*. Right:* $S_{\min}(t) = \min_j S(\overline{\mathbf{U}}_j(t))$*.*

density, low pressure, and large velocity, at an angle 45° with the x-axis.

In the computations, the domain is partitioned into $N \times N$ uniform rectangular cells with $N \in \{10, 20, 40, 80, 160\}$. For the P^3-based DG method, we take (only in this accuracy test) the time step-sizes as $\Delta t = 0.1\big(\frac{\Delta x}{2}\big)^{\frac{4}{3}}$ and $\Delta t = \frac{0.1}{3}\big(\frac{\Delta x}{2}\big)^{\frac{4}{3}}$ for the

third-order SSP-RK and SSP-MS time discretizations, respectively, so as to match the fourth-order accuracy of spatial DG discretization. Table 6.2 lists the numerical errors at $t = 0.2$ in the rest-mass density and the corresponding convergence rates for the P^k-based IRP DG methods ($k = 1, 2, 3$) at different grid resolutions. Similar to the 1D case and as also observed in [42, 24], the accuracy slightly degenerates for SSP-RK and $k \geq 2$. The desired full order of accuracy is observed for the SSP-MS time discretization, confirming that the IRP limiter itself does not lose the accuracy for smooth solutions as expected.

TABLE 6.2

Example 3: Errors at $t = 0.2$ in the rest-mass density for the proposed P^k-based DG methods ($k = 1, 2, 3$), with the SSP-RK or SSP-MS time discretization, at different spatial grid resolutions.

		SSP-RK				SSP-MS			
k	N	l^1 error	Order	l^2 error	Order	l^1 error	Order	l^2 error	Order
1	10	3.95e-2	–	4.80e-2	–	4.02e-2	–	4.80e-2	–
	20	7.62e-3	2.37	1.01e-2	2.24	7.54e-3	2.41	1.00e-2	2.26
	40	1.65e-3	2.21	2.25e-3	2.17	1.65e-3	2.20	2.24e-3	2.15
	80	3.85e-4	2.10	5.41e-4	2.05	3.84e-4	2.10	5.40e-4	2.05
	160	9.49e-5	2.02	1.34e-4	2.01	9.48e-5	2.02	1.34e-4	2.01
2	10	1.14e-2	–	1.46e-2	–	1.06e-2	–	1.34e-2	–
	20	3.90e-4	4.88	5.00e-4	4.87	3.80e-4	4.80	4.89e-4	4.78
	40	4.89e-5	3.00	6.21e-5	3.01	4.11e-5	3.21	5.47e-5	3.16
	80	6.55e-6	2.90	8.62e-6	2.85	4.90e-6	3.07	6.72e-6	3.03
	160	7.65e-7	3.10	1.22e-6	2.83	6.08e-7	3.01	8.38e-7	3.00
3	10	2.51e-4	–	3.75e-4	–	2.47e-4	–	3.70e-4	–
	20	1.82e-5	3.79	2.65e-5	3.82	1.81e-5	3.77	2.68e-5	3.79
	40	9.60e-7	4.24	1.43e-6	4.21	9.02e-7	4.33	1.30e-6	4.37
	80	6.55e-8	3.87	1.04e-6	3.78	5.56e-8	4.02	7.67e-8	4.08
	160	4.51e-9	3.86	9.14e-9	3.51	3.46e-9	4.01	4.71e-9	4.03

6.4. Example 4: Shock-bubble interaction. This example simulates the interaction between a planar shock wave and a light bubble within the domain $[0, 325] \times [-45, 45]$. The setup is the same as in [13, 44]. Initially, a left-moving relativistic shock wave is located at $x = 265$ with the left and right states given by

$$(\rho, \boldsymbol{v}, p)(x, y, 0) = \begin{cases} (1,\ 0,\ 0,\ 0.05), & x < 265, \\ (1.865225080631180,\ -0.196781107378299,\ 0,\ 0.15), & x > 265. \end{cases}$$

A light circular bubble with radius of 25 is initially centered at $(215, 0)$ in front of the initial shock wave. The fluid state within the bubble is $(\rho, \boldsymbol{v}, p)(x, y, 0) = (0.1358, 0, 0, 0.05)$. The reflective conditions are specified at both the top and bottom boundaries $\{y = \pm 45, 0 \leq x \leq 325\}$, and the inflow (resp., outflow) boundary condition is enforced at the right (resp., left) boundary.

In this simulation, we do not use any other nonoscillatory limiters, e.g., TVB or WENO limiters. Figure 6.3 shows the numerical results obtained by the fourth-order DG methods, with the BP limiter or the IRP limiter, respectively, on a mesh of 650×180 uniform cells. We observe serious oscillations developing near the top and bottom boundaries in the DG solution with only the BP limiter. However, if the IRP limiter is used, the undesirable oscillations are almost suppressed. From Figure 6.3(b), one can observe that the bubble interface, some small wave structures, and discontinuities are sharply resolved by the IRP DG method. To check the preservation of the minimum entropy principle, we plot the time evolution of the minimum specific entropy values of the DG solutions in Figure 6.4. It shows that the minimum stays

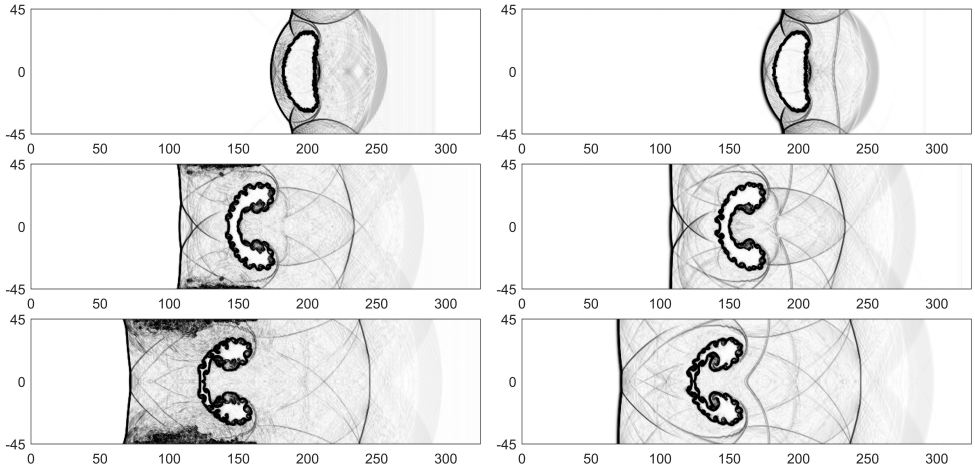

(a) With the BP limiter (b) With the IRP limiter

FIG. 6.3. *Example 4: Schlieren images of the density at $t = 180$, 360, and 450 (from top to bottom) obtained by the fourth-order DG methods on the mesh of 650×180 cells. (Here we do not use any other nonoscillatory limiters, e.g., TVB or WENO limiters.)*

the same for the DG scheme with the IRP limiter, which indicates that the minimum entropy principle is maintained, while the DG scheme with only the BP limiter does not preserve the principle.

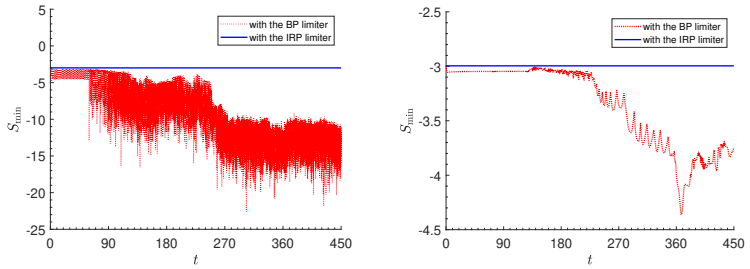

FIG. 6.4. *Example 4: Time evolution of $S_{\min}(t)$ for the DG solutions with the IRP limiter or with the BP limiter. Left: $S_{\min}(t) = \min_{K\in\mathcal{T}_h} \min_{\boldsymbol{x}\in\mathbb{X}_K} S(\mathbf{U}_h(\boldsymbol{x},t))$. Right: $S_{\min}(t) = \min_{K\in\mathcal{T}_h} S(\overline{\mathbf{U}}_K(t))$.*

6.5. Example 5: Two 2D Riemann problems. In this test, we simulate two Riemann problems of the 2D RHD equations, which have become benchmark tests for checking 2D RHD codes (cf. [13, 44, 34, 37, 2]).

The first Riemann problem was proposed in [34], with the initial data given by

$$(\rho, \boldsymbol{v}, p)(x, y, 0) = \begin{cases} (0.1, 0, 0, 20)^\top, & x > 0,\ y > 0, \\ (0.00414329639576, 0.9946418833556542, 0, 0.05)^\top, & x < 0,\ y > 0, \\ (0.01, 0, 0, 0.05)^\top, & x < 0,\ y < 0, \\ (0.00414329639576, 0, 0.9946418833556542, 0.05)^\top, & x > 0,\ y < 0, \end{cases}$$

where the left and lower initial discontinuities are contact discontinuities, and the upper and right are shock waves. Because the maximal value of the fluid velocity is very close to the speed of light ($c = 1$), nonphysical numerical solutions can be easily produced in the simulation, making this test challenging. For testing purposes, we do *not* use any other nonoscillatory limiters, e.g., TVB or WENO limiters. We evolve the solution up to $t = 0.8$ on the mesh of 200×200 cells within the domain $[-1, 1]^2$. The contours of $\log(\rho)$ are displayed in Figure 6.5, obtained by the fourth-order DG methods, with the BP or IRP limiter, respectively. Serious oscillations are observed in the DG solution with only the BP limiter, while if the IRP limiter is used (i.e., the entropy limiter is added), the oscillations are much reduced. The minimum entropy principle of the DG solution with the IRP limiter is validated in Figure 6.7. As the numerical solution is preserved in the set Ω_{S_0}, the IRP DG scheme exhibits good robustness in the simulation of such ultra-relativistic flow; the computed flow structures agree well with those reported in [34, 2]. We remark that if the BP or IRP limiter is turned off, the DG code would break down due to nonphysical numerical solutions.

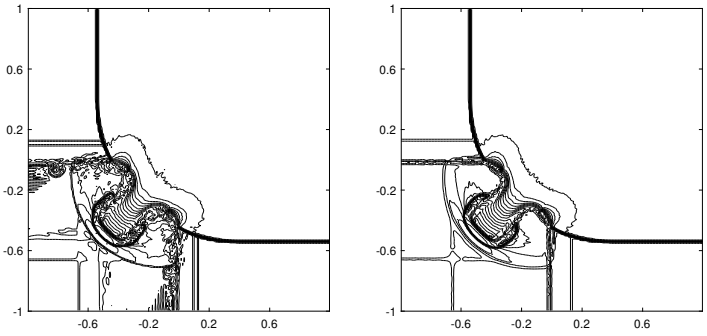

(a) With the BP limiter (without any other nonoscillatory limiters).

(b) With the IRP limiter (without any other nonoscillatory limiters).

FIG. 6.5. *The first 2D Riemann problem: The contours of $\log(\rho)$ at $t = 0.8$ obtained by the fourth-order DG methods with the BP limiter (left) or with the proposed IRP limiter (right), on the mesh of 200×200 cells. Eighteen equally spaced contour lines from -7.8981 to -2.5631 are displayed.*

The second Riemann problem was first proposed in [13], and its initial condition is given by

$$(\rho, \boldsymbol{v}, p)(x, y, 0) = \begin{cases} (0.035145216124503, 0, 0, 0.162931056509027)^\top, & x > 0,\ y > 0, \\ (0.1, 0.7, 0, 1)^\top, & x < 0,\ y > 0, \\ (0.5, 0, 0, 1)^\top, & x < 0,\ y < 0, \\ (0.1, 0, 0.7, 1)^\top, & x > 0,\ y < 0. \end{cases}$$

Figures 6.6(a) and 6.6(b) display the contours of $\log(\rho)$ at $t = 0.8$, obtained by the fourth-order DG methods, with the BP or IRP limiter, respectively, and without any nonoscillatory limiters, on the mesh of 200×200 cells within the domain $[-1, 1]^2$. For comparison and reference, we also present in Figures 6.6(c) the numerical result obtained by the fourth-order DG method with only the WENO limiter [44] on the

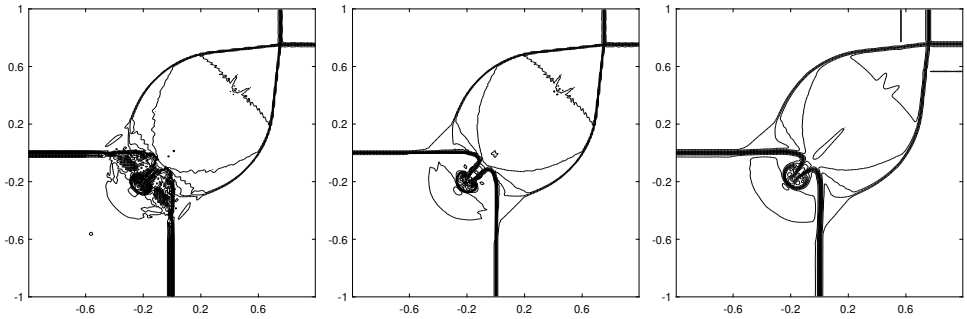

(a) BP limiter. (b) IRP limiter. (c) WENO limiter.

FIG. 6.6. *The second 2D Riemann problem: The contours of $\log(\rho)$ at $t = 0.8$ obtained by the fourth-order DG methods with three different limiters. Twenty equally spaced contour lines from -3.2533 to -0.426 are displayed.*

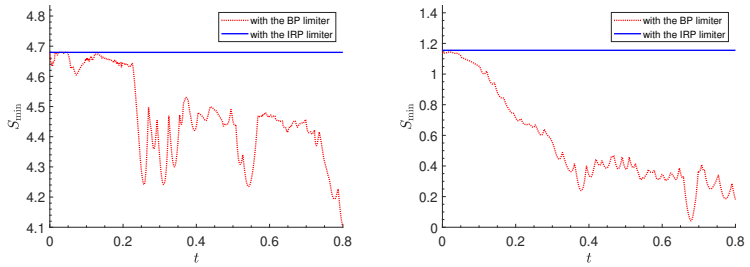

FIG. 6.7. *Example 5: Time evolution of $S_{\min}(t) = \min_{K\in\mathcal{T}_h} S(\overline{\mathbf{U}}_K(t))$ for the DG solutions with the IRP limiter or with the BP limiter. Left: for the first 2D Riemann problem. Right: for the second 2D Riemann problem.*

same mesh. (The WENO limiter is applied only within some "trouble" cells adaptively identified by the KXRCF indicator [19].) It is observed that the DG solution with only the BP limiter is oscillatory, while enforcing the minimum entropy principle by the IRP limiter does help to damp most of the oscillations. Although the WENO limiter may completely suppress the undesirable oscillations, the resulting numerical solution in Figure 6.6(c) is much more dissipative than that computed with the IRP limiter in Figure 6.6(b). Figure 6.7 shows the time evolution of the minimum specific entropy values of the DG solutions. One can see that the minimum remains the same for the DG scheme with the IRP limiter. This implies the preservation of minimum entropy principle, which, however, is not ensured by only using either the BP limiter or the WENO limiter.

The above numerical results have shown that the IRP limiter does help to preserve numerical solutions in the invariant domain Ω_{S_0} and to damp some numerical oscillations while keeping the high resolution. As pointed out in [16], the IRP limiter is still a mild limiter and may not completely suppress all the oscillations. For problems involving strong shocks, one may use the IRP limiter together with a nonoscillatory limiter (e.g., the WENO limiter) to sufficiently control all the undesirable oscillations while also preserving the invariant region Ω_{S_0}. Additional numerical examples, including a strong relativistic blast wave and two astrophysical jets, are presented in section SM7 of the supplementary material.

7. Conclusions. In this work, we extended Tadmor's minimum entropy principle (1.9) to the RHD equations (1.1) with the ideal EOS, and then developed high-order accurate IRP DG and finite volume schemes for RHD, which provably preserve a discrete minimum entropy principle as well as the intrinsic physical constraints (1.5). This was the first time that such a minimum entropy principle was explored for RHD at the continuous and discrete levels. Due to the relativistic effects, the specific entropy is a highly nonlinear function of the conservative variables and cannot be explicitly expressed. This led to some essential difficulties in this work which were not encountered in the nonrelativistic case. In order to address the difficulties, we first proposed a novel equivalent form of the invariant region. As a notable feature, all the constraints in this novel form became explicit and linear with respect to the conservative variables. This provided a highly effective approach to theoretically analyze the IRP property of numerical RHD schemes. We showed the convexity of the invariant region and established the generalized LF splitting properties via technical estimates. We rigorously proved that the first-order LF type scheme for the RHD equations satisfies a local minimum entropy principle and is IRP under a CFL condition. We then developed and analyzed provably IRP high-order accurate DG and finite volume methods for the RHD. Numerical examples confirmed that enforcing the minimum entropy principle could help to damp some undesirable numerical oscillations and demonstrated the robustness of the proposed high-order IRP DG schemes. The verified minimum entropy principle is an important property that can be incorporated into improving or designing other RHD schemes. In addition, the proposed novel analysis techniques can be useful for investigating or seeking other IRP schemes for the RHD or other physical systems.

REFERENCES

[1] D. S. Balsara and J. Kim, *A subluminal relativistic magnetohydrodynamics scheme with ADER-WENO predictor and multidimensional Riemann solver-based corrector*, J. Comput. Phys., 312 (2016), pp. 357–384.

[2] D. Bhoriya and H. Kumar, *Entropy-stable schemes for relativistic hydrodynamics equations*, Z. Angew. Math. Phys., 71 (2020), pp. 1–29.

[3] J. Duan and H. Tang, *High-order accurate entropy stable finite difference schemes for one-and two-dimensional special relativistic hydrodynamics*, Adv. Appl. Math. Mech., 12 (2020), pp. 1–29.

[4] S. Gottlieb, C.-W. Shu, and E. Tadmor, *Strong stability-preserving high-order time discretization methods*, SIAM Rev., 43 (2001), pp. 89–112, https://doi.org/10.1137/S003614450036757X.

[5] A. Gouasmi, K. Duraisamy, S. M. Murman, and E. Tadmor, *A minimum entropy principle in the compressible multicomponent Euler equations*, ESAIM: Math. Model. Numer. Anal., 54 (2020), pp. 373–389.

[6] F. Guercilena, D. Radice, and L. Rezzolla, *Entropy-limited hydrodynamics: a novel approach to relativistic hydrodynamics*, Comput. Astrophys. Cosmol., 4 (2017), 3.

[7] J.-L. Guermond, M. Nazarov, B. Popov, and I. Tomas, *Second-order invariant domain preserving approximation of the Euler equations using convex limiting*, SIAM J. Sci. Comput., 40 (2018), pp. A3211–A3239, https://doi.org/10.1137/17M1149961.

[8] J.-L. Guermond and B. Popov, *Viscous regularization of the Euler equations and entropy principles*, SIAM J. Appl. Math., 74 (2014), pp. 284–305, https://doi.org/10.1137/120903312.

[9] J.-L. Guermond and B. Popov, *Invariant domains and first-order continuous finite element approximation for hyperbolic systems*, SIAM J. Numer. Anal., 54 (2016), pp. 2466–2489, https://doi.org/10.1137/16M1074291.

[10] J.-L. Guermond and B. Popov, *Invariant domains and second-order continuous finite element approximation for scalar conservation equations*, SIAM J. Numer. Anal., 55 (2017), pp. 3120–3146, https://doi.org/10.1137/16M1106560.

[11] J.-L. Guermond, B. Popov, and I. Tomas, *Invariant domain preserving discretization-independent schemes and convex limiting for hyperbolic systems*, Comput. Methods Appl. Mech. Eng., 347 (2019), pp. 143–175.
[12] A. Harten, *On the symmetric form of systems of conservation laws with entropy*, J. Comput. Phys., 49 (1983), pp. 151–164.
[13] P. He and H. Tang, *An adaptive moving mesh method for two-dimensional relativistic hydrodynamics*, Commun. Comput. Phys., 11 (2012), pp. 114–146.
[14] X. Y. Hu, N. A. Adams, and C.-W. Shu, *Positivity-preserving method for high-order conservative schemes solving compressible Euler equations*, J. Comput. Phys., 242 (2013), pp. 169–180.
[15] Y. Jiang and H. Liu, *An invariant-region-preserving (IRP) limiter to DG methods for compressible Euler equations*, in Theory, Numerics and Applications of Hyperbolic Problems, II, Springer Proc. Math. Stat. 237, Springer, Cham, 2016, pp. 71–83.
[16] Y. Jiang and H. Liu, *Invariant-region-preserving DG methods for multi-dimensional hyperbolic conservation law systems, with an application to compressible Euler equations*, J. Comput. Phys., 373 (2018), pp. 385–409.
[17] Y. Jiang and H. Liu, *An invariant-region-preserving limiter for DG schemes to isentropic Euler equations*, Numer. Methods Partial Differential Equations, 35 (2019), pp. 5–33.
[18] B. Khobalatte and B. Perthame, *Maximum principle on the entropy and second-order kinetic schemes*, Math. Comput., 62 (1994), pp. 119–131.
[19] L. Krivodonova, J. Xin, J.-F. Remacle, N. Chevaugeon, and J. E. Flaherty, *Shock detection and limiting with discontinuous Galerkin methods for hyperbolic conservation laws*, Appl. Numer. Math., 48 (2004), pp. 323–338.
[20] Y. Lv and M. Ihme, *Entropy-bounded discontinuous Galerkin scheme for Euler equations*, J. Comput. Phys., 295 (2015), pp. 715–739.
[21] J. M. Martí and E. Müller, *Numerical hydrodynamics in special relativity*, Living Rev. Relativ., 6 (2003), 2003-7.
[22] J. M. Martí and E. Müller, *Grid-based methods in relativistic hydrodynamics and magnetohydrodynamics*, Living Rev. Comput. Astrophys., 1 (2015), 3.
[23] A. Mignone and G. Bodo, *An HLLC Riemann solver for relativistic flows–*I. *Hydrodynamics*, Mon. Not. R. Astron. Soc., 364 (2005), pp. 126–136.
[24] T. Qin, C.-W. Shu, and Y. Yang, *Bound-preserving discontinuous Galerkin methods for relativistic hydrodynamics*, J. Comput. Phys., 315 (2016), pp. 323–347.
[25] D. Radice, L. Rezzolla, and F. Galeazzi, *High-order fully general-relativistic hydrodynamics: new approaches and tests*, Class. Quantum Grav., 31 (2014), 075012.
[26] E. Tadmor, *Skew-selfadjoint form for systems of conservation laws*, J. Math. Anal. Appl., 103 (1984), pp. 428–442.
[27] E. Tadmor, *A minimum entropy principle in the gas dynamics equations*, Appl. Numer. Math., 2 (1986), pp. 211–219.
[28] K. Wu, *Design of provably physical-constraint-preserving methods for general relativistic hydrodynamics*, Phys. Rev. D, 95 (2017), 103001.
[29] K. Wu, *Positivity-preserving analysis of numerical schemes for ideal magnetohydrodynamics*, SIAM J. Numer. Anal., 56 (2018), pp. 2124–2147, https://doi.org/10.1137/18M1168017.
[30] K. Wu and C.-W. Shu, *A provably positive discontinuous Galerkin method for multidimensional ideal magnetohydrodynamics*, SIAM J. Sci. Comput., 40 (2018), pp. B1302–B1329, https://doi.org/10.1137/18M1168042.
[31] K. Wu and C.-W. Shu, *Provably positive high-order schemes for ideal magnetohydrodynamics: Analysis on general meshes*, Numer. Math., 142 (2019), pp. 995–1047.
[32] K. Wu and C.-W. Shu, *Entropy symmetrization and high-order accurate entropy stable numerical schemes for relativistic MHD equations*, SIAM J. Sci. Comput., 42 (2020), pp. A2230–A2261, https://doi.org/10.1137/19M1275590.
[33] K. Wu and C.-W. Shu, *Provably physical-constraint-preserving discontinuous Galerkin methods for multidimensional relativistic MHD equations*, Numer. Math., 148 (2021), pp. 699–741, https://doi.org/10.1007/s00211-021-01209-4.
[34] K. Wu and H. Tang, *High-order accurate physical-constraints-preserving finite difference WENO schemes for special relativistic hydrodynamics*, J. Comput. Phys., 298 (2015), pp. 539–564.
[35] K. Wu and H. Tang, *A direct Eulerian GRP scheme for spherically symmetric general relativistic hydrodynamics*, SIAM J. Sci. Comput., 38 (2016), pp. B458–B489, https://doi.org/10.1137/16M1055657.
[36] K. Wu and H. Tang, *Admissible states and physical-constraints-preserving schemes for relativistic magnetohydrodynamic equations*, Math. Models Methods Appl. Sci., 27 (2017),

pp. 1871–1928.
[37] K. Wu and H. Tang, *Physical-constraint-preserving central discontinuous Galerkin methods for special relativistic hydrodynamics with a general equation of state*, Astrophys. J. Suppl. Ser., 228 (2017), 3.
[38] Z. Xu, *Parametrized maximum principle preserving flux limiters for high order schemes solving hyperbolic conservation laws: One-dimensional scalar problem*, Math. Comp., 83 (2014), pp. 2213–2238.
[39] X. Zhang, *On positivity-preserving high order discontinuous Galerkin schemes for compressible Navier-Stokes equations*, J. Comput. Phys., 328 (2017), pp. 301–343.
[40] X. Zhang and C.-W. Shu, *On maximum-principle-satisfying high order schemes for scalar conservation laws*, J. Comput. Phys., 229 (2010), pp. 3091–3120.
[41] X. Zhang and C.-W. Shu, *On positivity-preserving high order discontinuous Galerkin schemes for compressible Euler equations on rectangular meshes*, J. Comput. Phys., 229 (2010), pp. 8918–8934.
[42] X. Zhang and C.-W. Shu, *A minimum entropy principle of high order schemes for gas dynamics equations*, Numer. Math., 121 (2012), pp. 545–563.
[43] X. Zhang, Y. Xia, and C.-W. Shu, *Maximum-principle-satisfying and positivity-preserving high order discontinuous Galerkin schemes for conservation laws on triangular meshes*, J. Sci. Comput., 50 (2012), pp. 29–62.
[44] J. Zhao and H. Tang, *Runge–Kutta discontinuous Galerkin methods with WENO limiter for the special relativistic hydrodynamics*, J. Comput. Phys., 242 (2013), pp. 138–168.